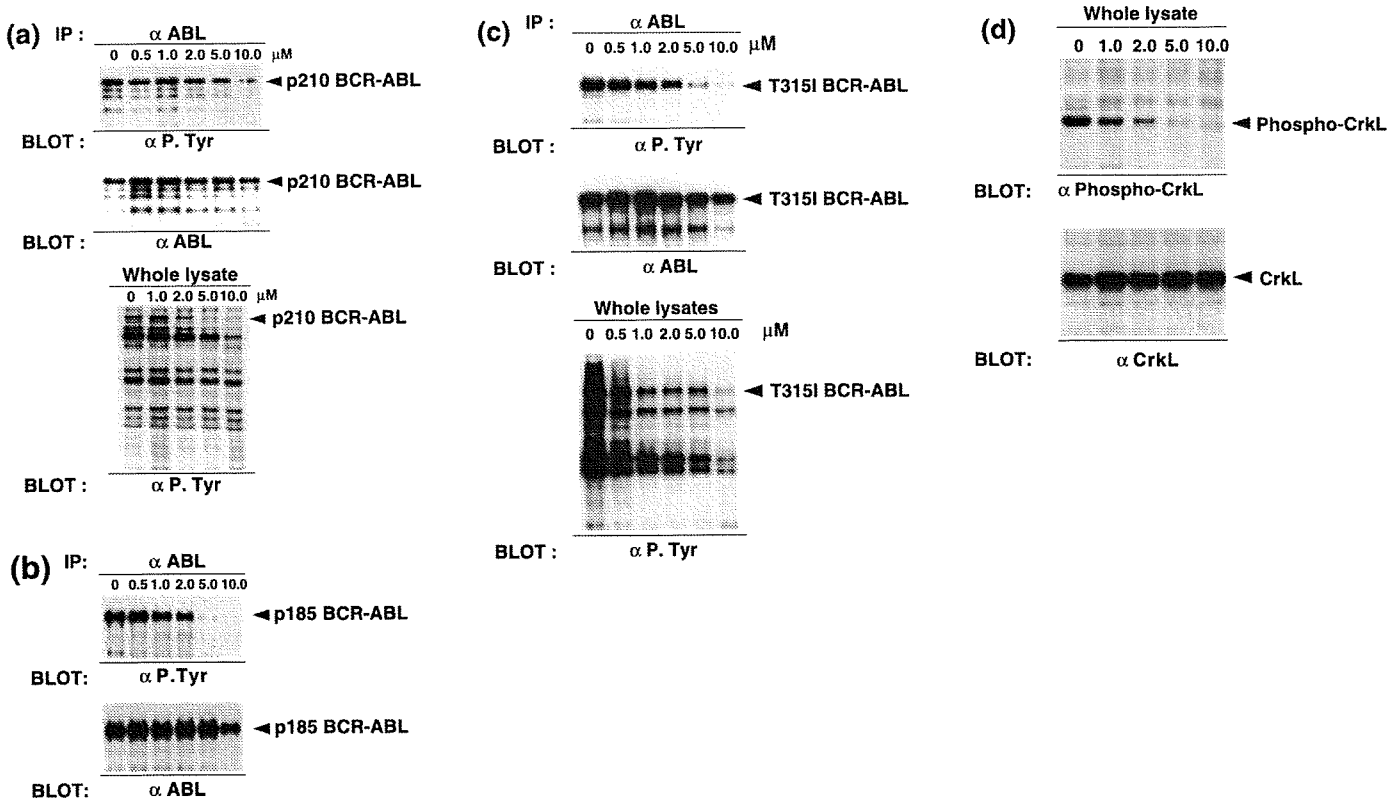

Fig. 2. Inhibition of BCR-ABL autophosphorylation by VE-465 in wild-type BCR-ABL- or T315I BCR-ABL-expressing leukemia cells. (a) K562, (b) BaF3 p185 BCR-ABL, and (c) BaF3 T315I BCR-ABL cells were cultured with the indicated concentrations of VE-465 for 24 h. The cell lysates were immunoprecipitated with anti-ABL antibody, and then the immunoprecipitates were immunoblotted with antiphosphotyrosine (P.Tyr) antibody (PY20), or anti-ABL antibody. (a,c lower panels) Whole-cell lysates were immunoblotted with anti-P.Tyr antibody. (d) BaF3 T315IBCR-ABL cells were cultured with the indicated concentrations of VE-465 for 24 h, and whole-cell lysates were immunoblotted with antiphospho-CrkL or anti-CrkL antibodies.

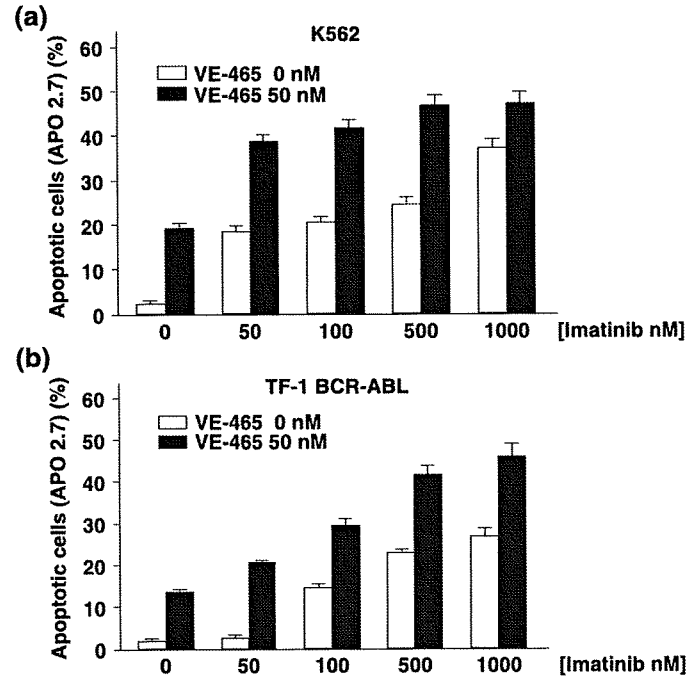

Fig. 3. Cotreatment of VE-465 and imatinib enhances the induction of apoptosis in BCR-ABL-transformed cells. (a) K562 and (b) TF-1BCR-ABL cells were cultured with the indicated concentrations of imatinib and dasatinib for 72 h, after which the percentage of apoptotic cells were determined using APO2.7 monoclonal antibody.

activity from leukemia cells expressing T315I BCR-ABL was also examined by immunoprecipitation after 6 h of treatment (Fig. 6c). Systemic administration of 50, 100, and 200 mg/kg VE-465 decreased the T315I BCR-ABL kinase activity compared to the control (Fig. 6c). These results demonstrate that VE-465 exhibits a desirable therapeutic index that can reduce the *in vivo* growth of wild-type and T315I mutant BCR-ABL-expressing cells in an efficacious manner.

Discussion

T315 serves as a gatekeeper residue that controls access to a hydrophobic region of the BCR-ABL enzymatic active site that is not contacted by ATP.[10,26] The T670I mutation in KIT and the T790M mutation in epidermal growth factor receptor are homologous to the T315I mutation in BCR-ABL, and all three mutations confer resistance to ATP-competitive kinase inhibitors.[27,28] Mutations of this residue can have profound effects on small-molecule binding in the context of different kinases, yet the mutations do not inactivate kinase function.[29] The T315I mutation in BCR-ABL confers resistance not only to imatinib, but also to all other second-generation ATP-competitive BCR-ABL inhibitors described so far, including dasatinib and nilotinib.[12,30] Clearly, the T315I mutation in BCR-ABL is predicted to be highly resistant to these agents and may drive the majority of acquired-resistance cases in the near future.

The Aurora kinase inhibitor MK-0457 is able to bind both wild-type and mutated BCR-ABL and has been reported to inhibit T315I BCR-ABL in primary patient cells at low micromolar concentrations.[31] Additionally, recent cocrystal studies have shown that this Y-shaped molecule engages the ABL kinase

doi: 10.1111/j.1349-7006.2008.00810.x

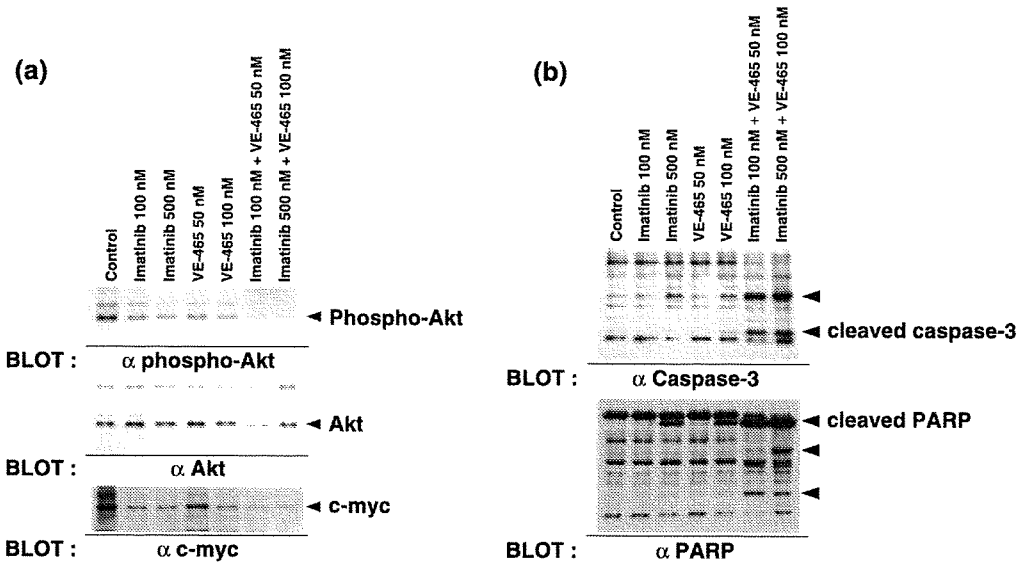

Fig. 4. Cotreatment with VE-465 and imatinib causes greater attenuation of phosphor-AKT and c-Myc, and induces caspase-3 and poly (ADP-ribose) polymerase (PARP) cleavage. (a) K562 cells were cultured with the indicated concentrations of VE-465 or imatinib for 24 h, and the cell lysates were immunoblotted with antiphospho-Akt, anti-Akt, or c-Myc antibodies. (b) K562 cells were cultured with the indicated concentrations of VE-465 or imatinib for 24 h, and the cell lysates were immunoblotted with anticaspase-3 or anti-PARP antibodies.

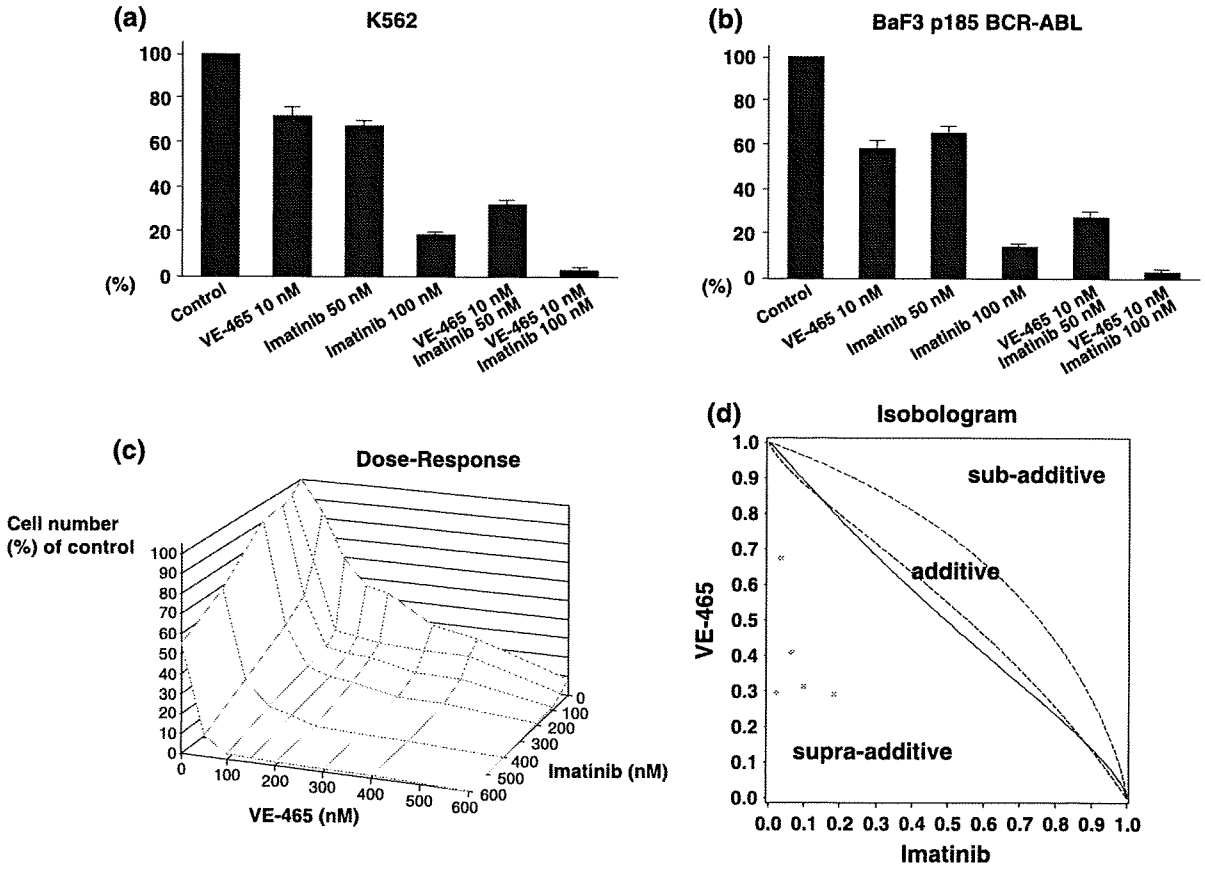

Fig. 5. Combination effects of VE-465 and imatinib in BCR-ABL-transformed cells. (a) K562 and (b) BaF3 p185BCR-ABL cells were grown in methylcellulose containing the indicated concentrations of VE-465 and imatinib. Colony counts were assessed on each individual sample at least twice, and the results are presented as average ± SD for colonies counted from triplicate plates under each condition. (c) The dose–response curve for VE-465 in combination with imatinib in K562 cells. (d) The isobologram shows the synergistic effect of simultaneous exposure to VE-465 and imatinib in K562 cells.

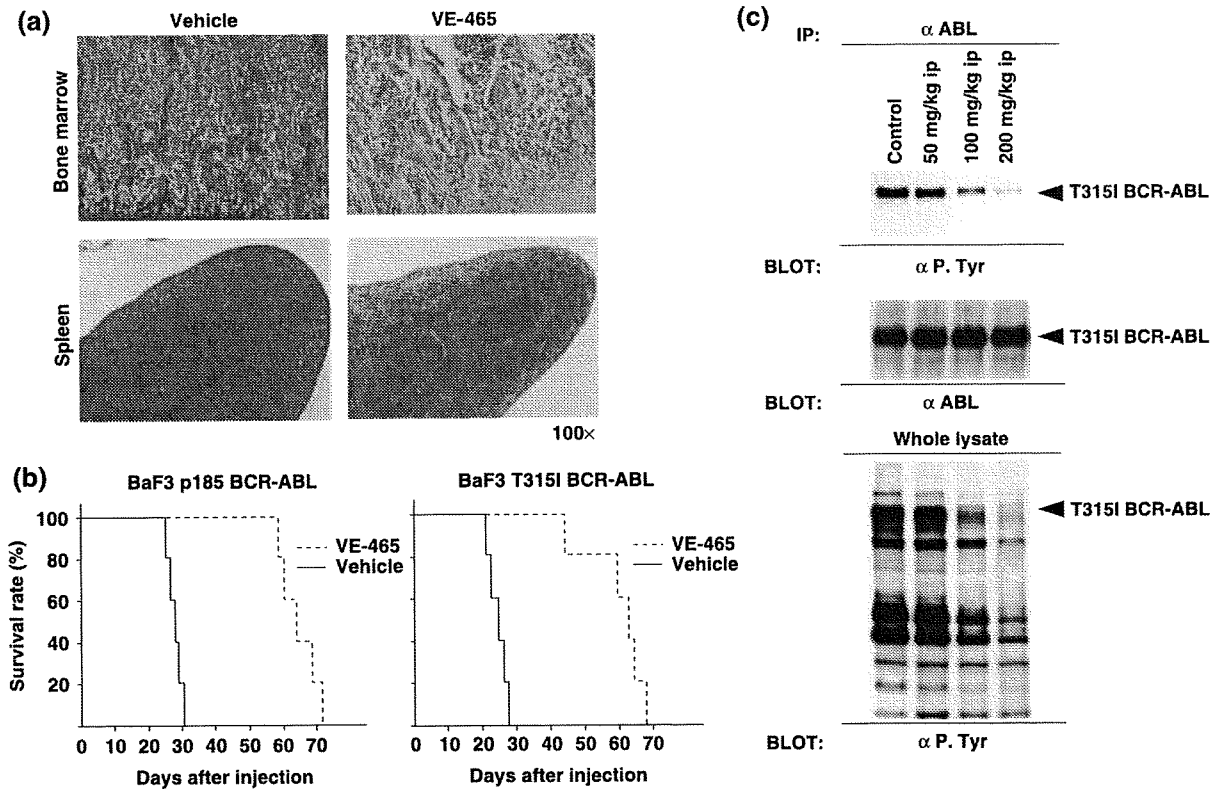

Fig. 6. *In vivo* efficacy of VE-465 in a mouse model of BCR-ABL-induced leukemia. (a) Histopathological analysis of bone marrow and spleen of mice injected with 10^6 BaF3 p185 BCR-ABL cells and treated with either VE-465 (75 mg/kg twice daily (b.i.d.); intraperitoneally (ip) for 14 days; 14 days resting) or vehicle alone. Magnification of photographs is indicated. (b) Survival of mice injected with 10^6 BaF3 p185 BCR-ABL cells or BaF3 T315I BCR-ABL cells and treated with either vehicle alone or VE-465 (75 mg/kg b.i.d.; ip for 14 days; 14 days resting). All mice that did not receive VE-465 died of a condition resembling acute leukemia by 28 days; nearly all mice treated with VE-465 survived for more than 56 days. (c) VE-465 inhibited T315I BCR-ABL kinase activity *in vivo*. Mice injected with BaF3 T315I BCR-ABL cells on day 20 with vehicle alone exhibited acute leukemia, characterized by splenomegaly and circulating blasts. The T315I BCR-ABL kinase activity of leukemia cells from the spleen was examined by immunoprecipitation after 6 h VE-465 treatment. Systemic administration of 100 or 200 mg/kg VE-465 decreased T315I BCR-ABL kinase activity compared to the control. P. Tyr, phosphotyrosine.

domain in such a way that a close encounter with the gatekeeper residue is avoided, explaining why the compound is able to accommodate the substitution of threonine with isoleucine without any significant decrease in binding affinity.[31] MK-0457 is currently undergoing a phase I clinical trial in BCR-ABL-positive leukemias, and encouraging responses in patients harboring the T315I mutation have been reported.[18] However, a phase II clinical trial in the specific setting of T315I-positive leukemia revealed several non-hematological toxicities. Therefore, the development of related compounds will be important for further clinical studies.

In the present study, we investigated the activity of a novel Aurora kinase inhibitor, VE-465, against wild-type and T315I mutant BCR-ABL-expressing leukemia cells. VE-465 inhibited the proliferation of K562 cells, BaF3 p185BCR-ABL cells, and BaF3 T315IBCR-ABL cells with IC_{50} values ranging from 50 to 500 nM (Fig. 1b–d). Further, VE-465 ranging from 200 to 500 nM caused accumulation of cells in G_2/M arrest (Fig. 1f). These results suggest that the growth-inhibitory effect of VE-465 on BCR-ABL-expressing cells is caused by Aurora kinase inhibition. VE-465 inhibited wild-type and T315I mutant BCR-ABL autophosphorylation with IC_{50} values ranging from 2.0 to 5.0 μM (Figs 1,2). However, it is important to note that systemic administration of 100 and 200 mg/kg VE-465 decreased T315I BCR-ABL autophosphorylation compared with the control (Fig. 6c). These results suggest that systemic administration of 100 or 200 mg/kg VE-465 in mice may achieve low micromolar plasma VE-465 concentrations.

We have also demonstrated that combined treatment with VE-465 and imatinib is significantly more active than either agent alone against K562 and BaF3 p185BCR-ABL cells (Figs 3–5). Indeed, the isobologram indicated the synergistic effect of simultaneous exposure to VE-465 and imatinib in K562 cells (Fig. 5d). VE-465 and imatinib and the combination of these compounds suppress the expression of c-Myc protein differently (Fig. 4a). Recently, Samanta *et al.* demonstrated that signal transduction by the BCR-ABL–Jak2 network results in phosphorylation of Akt, which leads to stabilization of c-Myc and activates nuclear factor (NF)-κB to cause elevation of c-Myc transcripts.[32] Compared with treatment with either agent alone, cotreatment with VE-465 and imatinib caused more attenuation of the levels of phosho-Akt and c-Myc (Fig. 4a). A recent study also showed that Aurora kinase inhibition by MK-0457 downregulated NF-κB in the human lung cell line A549.[33] Further data are required to resolve the combined effect of VE-465 and imatinib in BCR-ABL transformed cells.

Combinations of different BCR-ABL kinase inhibitors, including imatinib, dasatinib, and VE-465, might be effective in reducing the occurrence of drug-resistant mutants. Interestingly, new evidence has shown that sequential ABL kinase inhibitor therapy in CML selects for compound drug-resistant BCR-ABL mutations, demonstrating the potential hazards of sequential kinase inhibitor therapy and suggesting a beneficial effect of combination therapy.[34] In the case of imatinib-resistant leukemia, because of the nature of resistant mechanisms, such as the emergence of BCR-ABL kinase domain point mutations, it will

doi: 10.1111/j.1349-7006.2008.00810.x

likely be of significant clinical benefit to simultaneously administer more than one BCR-ABL inhibitor to patients as a way to suppress the development of drug-resistant mutants.

In conclusion, strategies to effectively control resistance mediated by the T315I mutation represent the next major frontier in the targeted treatment of CML. Agents such as VE-465, coupled with existing ABL kinase inhibitors, may help improve survival in advanced-phase CML. Strategies aimed at greater frontline disease eradication and suppression of resistance are needed, most of which depend on further research into combination chemotherapy and next-generation BCR-ABL kinase inhibitors that are active against the T315I BCR-ABL mutant.

References

1 Druker BJ, Tamura S, Buchdunger E *et al.* Effects of a selective inhibitor of the Abl tyrosine kinase on the growth of BCR-ABL positive cells. *Nature Med* 1996; **5**: 561–6.
2 Druker BJ, Talpaz M, Resta DJ *et al.* Efficacy and safety of a specific inhibitor of the BCR-ABL tyrosine kinase in chronic myeloid leukemia. *N Engl J Med* 2001; **344**: 1031–7.
3 O'Brien SG, Guilhot F, Larson RA *et al.* Imatinib compared with interferon and low-dose cytarabine for newly diagnosed chronic-phase chronic myeloid leukemia. *N Engl J Med* 2003; **348**: 994–1004.
4 Druker BJ, Sawyers CL, Kantarjian H *et al.* Activity of a specific inhibitor of the BCR-ABL tyrosine kinase in the blast crisis of chronic myeloid leukemia and acute lymphoblastic leukemia with the Philadelphia chromosome. *N Engl J Med* 2001; **344**: 1038–42.
5 Talpaz M, Silver RT, Druker BJ *et al.* Imatinib induces durable hematologic and cytogenetic responses in patients with accelerated phase chronic myeloid leukemia: results of a phase 2 study. *Blood* 2002; **99**: 1928–37.
6 Hughes TP, Kaeda J, Bransford S *et al.* Frequency of major molecular responses to imatinib or interferon α plus cytarabine in newly diagnosed chronic myeloid leukemia. *N Engl J Med* 2003; **349**: 1423–32.
7 Shah NP, Nicoll JM, Nagar B *et al.* Multiple BCR-ABL kinase domain mutations confer polyclonal resistance to the tyrosine kinase inhibitor imatinib (STI571) in chronic phase and blastic crisis chronic myeloid leukemia. *Cancer Cell* 2002; **2**: 117–25.
8 Hochhaus A, Kreil S, Corbin AS *et al.* Molecular and chromosomal mechanisms of resistance to imatinib (STI571) therapy. *Leukemia* 2002; **16**: 2190–6.
9 Corbin AS, La Rosee P, Stroffrengen EP, Druker BJ, Deininger MW. Several BCR-ABL kinase domain mutants associated with imatinib mesylate resistance remain sensitive to imatinib. *Blood* 2003; **101**: 4611–14.
10 Schindler T, Bormann W, Pellicena P, Miller WT, Clarkson B, Kuriyan J. Structural mechanism for STI571 inhibition of Abelson tyrosine kinase. *Science* 2000; **289**: 1938–42.
11 Roumiantsev S, Shah NP, Gorre ME *et al.* Clinical resistance to the tyrosine kinase inhibitor STI571 in chronic myeloid leukemia by mutation of Tyr-253 in the Abl kinase domain P-loop. *Proc Acad Sci USA* 2002; **99**: 10 700–5.
12 Shah NP, Tran C, Lee FY, Chen P, Norris D, Sawyers CL. Overriding imatinib resistance with a novel ABL kinase inhibitor. *Science* 2004; **305**: 399–401.
13 Tauchi T, Ohyashiki K. The second generation of BCR-ABL tyrosine kinase inhibitors. *Int J Hemato* 2006; **83**: 294–300.
14 Nicolini FE, Corm S, Le QH *et al.* Mutation status and clinical outcome of 89 imatinib mesylate-resistant chronic myelogenous leukemia patients: a retrospective analysis from the French intergroup of CML. *Leukemia* 2006; **20**: 1061–6.
15 Noble ME, Endicott JA, Johnson LN. Protein kinase inhibitors: insights into drug design from structure. *Science* 2004; **303**: 1800–5.
16 Harrington EA, Bebbington D, Moore J *et al.* VX-680, apotent and selective small-molecule inhibitor of the Aurora kinases, suppresses tumor growth *in vivo*. *Nature Med* 2004; **10**: 262–7.
17 Carter TA, Wodicka LM, Shah NP *et al.* Inhibition of drug-resistant mutants of ABL, KIT, and EGF receptor kinases. *Proc Natl Acad Sci USA* 2005; **102**: 11 011–16.
18 Giles F, Cortes J, Jones D, Bergstrom D, Kantarjian H, Freedman SJ. MK-0457, a novel kinase inhibitor, is a active in patients with chronic myeloid leukemia or acute lymphocytic leukemia with the T315I BCR-ABL mutation. *Blood* 2007; **109**: 500–2.
19 Young MA, Shah NP, Chao LH *et al.* Structure of the kinase domain of an imatinib-resistant Abl mutant in complex with the aurora kinase inhibitor VX-680. *Proc Natl Acad Sci USA* 2006; **66**: 1007–14.
20 Nunoda K, Tauchi T, Takaku T *et al.* Identification and functional signature of genes regulated by structurally different ABL kinase inhibitors. *Oncogene* 2007; **26**: 4179–88.
21 Komatsu N, Watanabe T, Uchida M *et al.* A member of Forkhead transcription factor FKHRL1 is a downstream effector of STI571-induced cell cycle arrest in BCR-ABL-expressing cells. *J Biol Chem* 2003; **278**: 6411–19.
22 Nakajima A, Tauchi T, Sashida G *et al.* Telomerase inhibition enhances apoptosis in human acute leukemia cells: possible of antitelomerase therapy. *Leukemia* 2003; **14**: 560–7.
23 Tauchi T, Feng GS, Shen R *et al.* SH2-containing phosphotyrosine phosphatase Syp is a target of p210bcr-abl tyrosine kinase. *J Biol Chem* 1994; **269**: 15 381–7.
24 Kano Y, Akutsu M, Tsunoda S *et al. In vitro* cytotoxic effects of a tyrosine kinase inhibitor STI571 in combination with commonly used antileukemic agents. *Blood* 2001; **97**: 1999–2007.
25 Tauchi T, Shin-ya K, Sashida G *et al.* Activity of a novel G-quadruplex-interactive telomerase inhibitor, telomestatin (SOT-095), against human leukemia cells: involvement of ATM-dependent DNA damage response pathways. *Oncogene* 2003; **22**: 5338–47.
26 Gorre ME, Mohammed M, Ellwood K *et al.* Clinical resistance to STI-571 cancer therapy caused by BCR-ABL gene mutation or amplification. *Science* 2001; **293**: 876–80.
27 Tamborini E, Bonadiman L, Greco A *et al.* A new mutation in the KIT ATP pocket causes acquired resistant to imatinib in a gastrointestinal stromal tumor patients. *Gastroenterology* 2004; **127**: 294–9.
28 Kobayashi S, Boggon TJ, Dayaram T *et al.* EGFR mutation and resistance of non-small-cell lung cancer to gefitinib. *N Engl J Med* 2005; **352**: 786–92.
29 Daub H, Specht K, Ullrich A. Strategies to overcome resistance to targeted protein kinase inhibitors. *Nat Rev Drug Discov* 2004; **12**: 1001–10.
30 Weisberg E, Manley PW, Breitenstein W *et al.* Characterization of AMN107, a selective inhibitor of native and mutant BCR-ABL. *Cancer Cell* 2005; **7**: 129–41.
31 Young MA, Shah NP, Chao LH *et al.* Structure of the kinase domain of an imatinib-resistant ABL mutant in complex with the Aurora kinase inhibitor VX-680. *Cancer Res* 2006; **66**: 1007–14.
32 Samanta AK, Lin H, Sun T *et al.* Janus Kinase 2: a critical target in chronic myelogenous leukemia. *Cancer Res* 2006; **66**: 6468–72.
33 Sun C, Chan F, Briassouli P *et al.* Aurora kinase inhibition downregulates NF-κB and sensitises tumor cells to chemotherapeutic agents. *Biochem Biophys Res Commun* 2007; **352**: 220–5.
34 Shah NP, Skaggs BJ, Branford S *et al.* Sequential ABL kinase inhibitor therapy selects for compound drug-resistant BCR-ABL mutations with altered oncogenic potency. *J Clin Invest* 2007; **117**: 2562–9.

[Autophagy 4:5, 629-640; 1 July 2008]; ©2008 Landes Bioscience

Research Paper

Vitamin K2 induces autophagy and apoptosis simultaneously in leukemia cells

Tomohisa Yokoyama,[1,5,†] Keisuke Miyazawa,[1,†,*] Munekazu Naito,[2] Juri Toyotake,[1] Testuzo Tauchi,[1] Masahiro Itoh,[2] Akira Yuo,[3] Yuho Hayashi,[4] Maria-Magdalena Georgescu,[4] Yasuko Kondo,[5] Seiji Kondo[5] and Kazuma Ohyashiki[1]

[1]First Department of Internal Medicine; Tokyo Medical University; [2]Department of Anatomy; Tokyo Medical University; Tokyo, Japan;[3]Department of Hematology; Research Institute; International Medical Center of Japan; Tokyo, Japan; [4]Department of Neuro-Oncology and [5]Department of Neurosurgery; The University of Texas MD Anderson Cancer Center; Houston, Texas USA

[†]These authors contributed equally to this work.

Key words: vitamin K2, autophagy, apoptosis, leukemia, acute myeloid leukemia, bcl-2

Vitamin K2 (menaquinone-4: VK2) is a potent inducer for apoptosis in leukemia cells in vitro. HL-60*bcl-2* cells, which are derived from a stable transfectant clone of the human *bcl-2* gene into the HL-60 leukemia cell line, show 5-fold greater expression of the Bcl-2 protein compared with HL-60*neo* cells, a control clone transfected with vector alone. VK2 induces apoptosis in HL-60*neo* cells, whereas HL-60*bcl-2* cells are resistant to apoptosis induction by VK2 but show inhibition of cell growth along with an increase of cytoplasmic vacuoles during exposure to VK2. Electron microscopy revealed formation of autophagosomes and autolysosomes in HL-60*bcl-2* cells after exposure to VK2. An increase of acid vesicular organelles (AVOs) detected by acridine orange staining for lysosomes as well as conversion of LC3B-I into LC3B-II by immunonoblotting and an increased punctuated pattern of cytoplasmic LC3B by fluorescent immunostaining all supported induction of enhanced autophagy in response to VK2 in HL-60*bcl-2* cells. However, during shorter exposure to VK2, the formation of autophagosomes was also prominent in HL-60*neo* cells although nuclear chromatin condensations and nuclear fragments were also observed at the same time. These findings indicated the mixed morphologic features of apoptosis and autophagy. Inhibition of autophagy by either addition of 3-methyladenine, siRNA for Atg7, or Tet-off Atg5 system all resulted in attenuation of VK2-incuded cell death, indicating autophagy-mediated cell death in response to VK2. These data demonstrate that autophagy and apoptosis can be simultaneously induced by VK2. However, autophagy becomes prominent when the cells are protected from rapid apoptotic death by a high expression level of Bcl-2.

*Correspondence to: Keisuke Miyazawa; First Department of Internal Medicine; Tokyo Medical University; 6-7-1, Nishishinjuku; Shinjuku-ku, Tokyo 160-0023 Japan; Tel.: +81.3.3342.6111, ext. 5985; Fax: +81.3.5381.6651; Email: miyazawa@tokyo-med.ac.jp

Submitted: 09/13/07; Revised: 03/19/08; Accepted: 03/20/08

Previously published online as an *Autophagy* E-publication:
http://www.landesbioscience.com/journals/autophagy/article/5941

Introduction

The vitamin K family contains both natural and synthetic forms, the former including phytonadione (VK1) and the menaquinone series (VK2), and the latter including menadione (VK3). Recent studies have reported that VK2 can exert cell growth-inhibitory effects in various human cancer cells including leukemia, lung cancer and hepatocellular carcinoma (HCC) cells.[1-5] We previously reported that this cytotoxic effect of VK2 appears to be selective to leukemic blasts with almost no effects on normal hematopoietic progenitor cells.[2,6] This suggests a therapeutic advantage for using VK2 in therapy for leukemia. Several recent clinical trials demonstrated that oral administration of VK2 reduced leukemic blasts in acute myeloid leukemia (AML) and improvement of cytopenias in myelodysplastic syndromes (MDS), and also decreased the development and recurrence rates of HCC, thus improving the overall survival of patients with HCC.[7-10] Although the precise mechanism of how VK2 exerts its growth-inhibitory effects in cancer cells has not been determined, VK2 has been reported to be a potent inducer of apoptosis in various tumor cells including leukemic cells in vitro.[2,3,11-15]

Apoptosis is an evolutionally conserved, orchestrated cell-death process characterized by membrane-blebbing, DNA fragmentation, and the formation of distinct apoptotic bodies that contain components of the dead cell.[16,17] This process occurs without membrane breakdown and does not elicit an inflammatory response. Apoptotic bodies are eventually removed by phagocytic cells. Central to this apoptotic process are a group of caspases, which effect the destruction of the cell in an orderly fashion.[17] Extensive evidence suggests that therapeutic effects of various anti-cancer reagents and of radiation are mediated though apoptosis of cancer cells.[18] However, another type of caspase-independent cell death designated autophagic cell death has recently been suggested in some cancer cells in response to anticancer therapy.[19-22]

Autophagy is also an evolutionally conserved membrane trafficking process that leads to degradation of cytosolic proteins and organelles by lysosomes.[23,24] Cytosol and organelles such as mitochondria and endoplasmic reticulum are engulfed into double-membraned vesicles called autophagosomes. Fusion subsequently occurs between the

autophagosomes and lysosomes to form autolysosomes in which the cargo of the autophagosome is degraded by lysosomal hydrolases. Autophagy is induced above basal levels in response to nutrient deprivation or trophic factor withdrawal, and it sustains metabolism through the targeted catabolism of long-lived proteins. Thus, autophagy acts as a self-limited survival mechanism.[23,24] A group of genes known as Atg genes, which are conserved from yeast to humans, have been found to regulate autophagy.[25] A number of studies have reported that autophagy is activated in cancer cells derived from breast, colon, prostate and brain in response to various anticancer therapies.[21,22] Since inhibition of autophagy results in suppression of cancer cell death by anti-cancer reagents, autophagy is suggested to be a potential contributor to non-apoptotic programmed cell death.[19,21] When cell death involves autophagy, it is now designated as type II programmed cell death (PCD) or autophagic cell death, in contrast to apoptosis, which is referred to as type I PCD.[19,21] The morphological and biochemical features of autophagic cell death and apoptosis are generally distinct. In autophagic cell death, unlike apoptotic cell death, caspases are not activated, and neither DNA degradation nor nuclear fragmentation is apparent. Instead, autophagic cell death is characterized by degradation of the Golgi apparatus, polyribosomes and endoplasmic reticulum before nuclear destruction, whereas these organelles are preserved in apoptosis.[19,21] However, the involvement of autophagy in programmed cell death is still controversial, probably because the molecule(s) which execute cell death in autophagy have not been identified.[20-22]

We have previously reported that overexpression of Bcl-2 in a leukemia cell line resulted in resistance against VK2-induced apoptosis but these cells still underwent differentiation via G_1 arrest.[12] In addition, downregulation of Bcl-2 was reported to cause autophagy of HL-60 cells in a caspase-independent manner.[26] It has also been reported that Bcl-2 negatively regulates Beclin 1-depemdent autophagy and Beclin 1-dependent autophagic cell death.[27] All these data suggest the involvement of Bcl-2 in some autophagic signaling and also imply some direct or indirect interaction between mitochondria and lysosomes.[28]

In the present study, we investigated whether autophagy is involved in VK2-induced leukemic cell death using subclones of HL-60 cell line with higher and lower expression levels of the Bcl-2 protein. Our data demonstrated that both autophagy and apoptosis are simultaneously induced after VK2 treatment, but autophagy become more evident and detectable when the cells are protected from apoptosis.

Results

Bcl-2 abolished VK2-induced apoptosis but had little effect on VK2-induced growth inhibition in HL-60 cells. We have reported that treating the primary cultured leukemic cells and leukemic cell lines with 1–10 μM of VK2 for 48 to 96 hr induces apoptosis in vitro, and that the expression levels of Bcl-2 determine whether the leukemic cells to undergo apoptosis or differentiation.[2,12]

Immunoblotting with anti-Bcl-2 mAb revealed that HL-60*bcl-2* cells, which are stably transfected with human *bcl-2*, expresse Bcl-2 at a five-fold higher level than HL-60*neo* control cells (Fig. 1A). There was no difference in growth rate, morphology, and antigen expressions among the parental HL-60, HL-60*neo*, and HL-60*bcl-2* cells (data not shown). Thereafter, cell growth inhibition was assessed after 96-hr exposure to VK2 (menaquinone-4) at various concentrations. As shown in Figure 1B, VK2 inhibited HL-60 cell growth in a dose-dependent manner. HL-60*bcl-2* cells were less sensitive as compared with HL-60*neo* cells; the concentrations for the 50% growth inhibition (IC_{50}) were 6 μM for HL-60*neo* and 14 μM for HL-60*bcl-2* cells, respectively.[12] As previously reported in other leukemic cell lines and primary cultured leukemic cells,[2,11,13] treatment with 10 μM of VK2 for 72 hr potently induced apoptosis of HL-60*neo* cells as assessed by morphology, depolarization of mitochondrial membrane potential, and annexin V staining (Fig. 1C–E). In contrast, apoptosis induction by VK2 treatment was significantly suppressed in HL-60*bcl-2* cells (Fig. 1D and E), although the inhibition of cell growth was still detectable, and extended exposure to VK2 induced cell death in HL-60*bcl-2* cells (Fig. 1B). We therefore investigated whether the autophagy or non-apoptotic cell death occurred in HL-60*bcl-2* cells after treatment with VK2.

Induction of autophagy in HL-60neo/*bcl-2* cells by VK2. Since cytoplasmic vesicles became evident in HL-60*bcl-2* cells after treatment with VK2 (Fig. 1C), we first performed electron microscopy to determine whether VK2 induces autophagy in HL-60*bcl-2* cells and compared the results with those obtained with HL-60*neo* cells. As shown in Figure 2A (upper right), the nuclear degeneration and multiple chromatin bodies, which are characteristic features for the cells undergoing apoptosis, were observed in HL-60*neo* cells treated with 10 μM of VK2 for 72 hr. In contrast, numerous autophagic vacuoles and empty vacuoles were observed in HL-60*bcl-2* cells under the same conditions (Fig. 2B; upper right and lower). Most of the autophagosomes contained lamellar structures with residual digested materials. These results indicated that HL-60*bcl-2* cells treated with VK2 undergo autophagy.

It was previously reported that during amino acid starvation, LC3 becomes localized to form isolated membrane following formation of autophagosome membranes.[34] Therefore detection of the punctuated pattern of cytosolic LC3 indicates the involvement of LC3 for autophagosome formation. This phenomenon has been used as method for monitoring autophagy.[35] To further confirm the involvement of LC3 in VK2-induced autophagy, we performed fluorescent immunocytostaining of HL-60neo/*bcl-2* cells with anti-LC3B Ab and subsequent counter staining with DAPI for the detection of nuclei. As shown in Figure 3A and B, untreated HL-60*neo* and HL-60*bcl-2* cells both showed diffuse distribution of green fluorescence and no fragmented nuclei, whereas treatment with VK2 increased the punctuated pattern of LC3B in HL-60*bcl-2* cells, representing autophagic vacuoles. HL-60*neo* cells with fragmented nuclei showed no punctuated pattern of LC3B. However, in a minor population of HL-60*neo* cells without fragmented nuclei, the punctuated pattern of LC3B staining was detected. Among the cells without nuclear fragments during 72 hr-treatment with 10 μM of VK2, the percentage showing the punctuated pattern of LC3B increased in HL-60*neo* cells as well as HL-60*bcl-2* cells (Fig. 3B). This indicates that autophagy can be detected not only HL-60*bcl-2*cells but also HL-60*neo* cells. Within 48 hrs of exposure to VK2, autophagy induction was rather prominent in HL-60*neo* cells as compared with HL-60*bcl-2* cells.

Simulations induction of both apoptosis and autophagy in HL-60 cells after treatment with VK2. The data shown above suggested that both autophagy and apoptosis appear to be induced in response to VK2 in HL-60*neo* cells. For semi-quantitative assessment of the induction of autophagy, we examined the development of acid

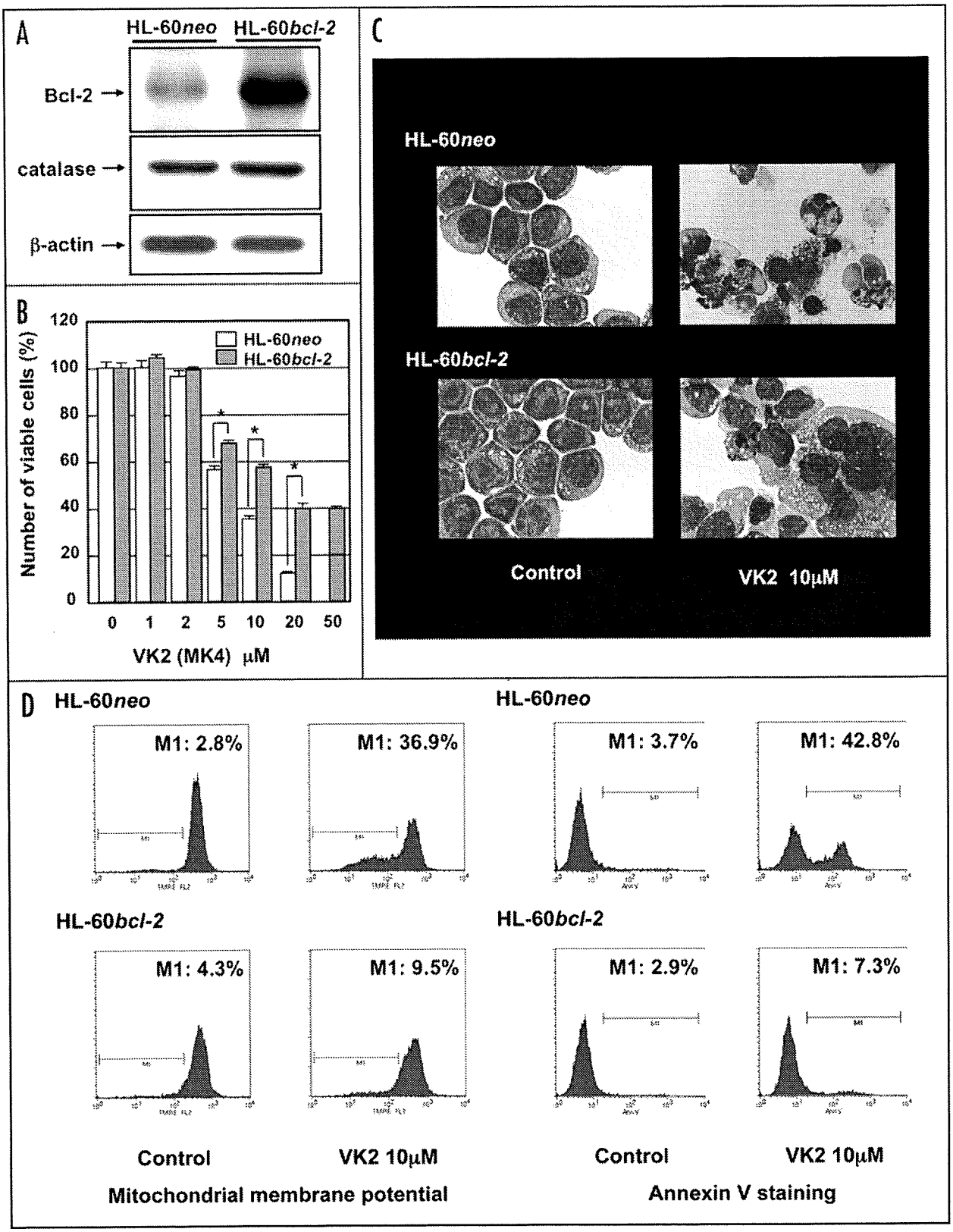

Figure 1. Inhibition of cell growth and induction of apoptosis after treatment with VK2 in HL-60 cells. (A) Expression of Bcl-2 and catalase in HL-60*neo* and HL-60*bcl-2* cells: Cellular proteins were lysed and separated by 15% SDS-PAGE for Bcl-2 and 11.25% SDS-PAGE for catalase and β-actin, and immunoblotted with anti-human Bcl-2 mAb, anti-catalase rabbit mAb, or anti-β-actin Ab, respectively. (B) Cell growth inhibition in response to VK2 in HL-60*neo*/HL-60*bcl-2* cells: Cells were cultured in the presence of various concentrations of VK2 (0.1–50 μM) for 72 hr. The number of cells was assessed with the WST cell counting kit as described in Materials and Methods. Cell growth is expressed as a ratio to the untreated control cells. *$p < 0.001$. After 72 hr exposure to 10 μM of VK2, HL-60*neo* and HL-60*bcl-2* cells were processed for (C) May-Grünwald-Giemsa staining for assessment of morphologic changes (original magnification x1,000), and flow cytometry for (D) mitochondrial membrane potential using TMRE, and (E) Annexin V staining as described in Materials and Methods.

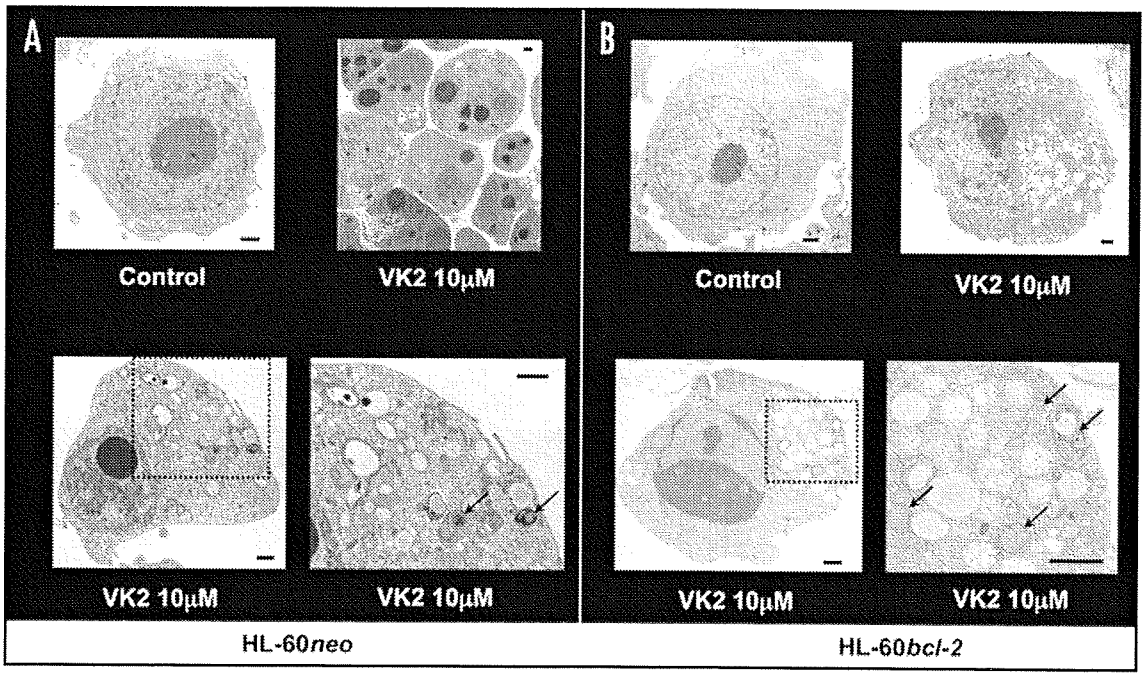

Figure 2. Ultrastructural features of HL-60*neo*/HL-60*bcl-2* cells after exposure to VK2. HL-60*neo*/HL-60*bcl-2* cells treated with or without 10 μM of VK2 for 72 hr. Then the cells were fixed, and the electron microscopy was performed. (A) HL-60*neo* cells: upper left; untreated control cells, upper right and lower; VK2-treated cells. (B) HL-60*bcl-2* cells: upper left; untreated cells, upper right and lower; VK2-treated cells. Arrows indicate autolysosomes.

vesicular organelles (AVOs) with acridine orange staining followed by flow cytometry as previously reported.[29] Figure 3C demonstrates that treatment with 10 μM VK2 increased the bright red fluorescence intensity (y-axis) from 4.8% to 46.8% in HL-60*neo* cells and that from 4.7% to 47.3% in HL-60*bcl-2* cells, respectively. These data further support the conclusion that autophagy is induced as well as apoptosis in HL-60*neo* cells. By increasing the concentration of VK2 at 20 μM, the intensity of AVO decreased to 31.5% in HL-60*neo* cells, indicating suppression of autophagy. Under these conditions apoptosis masked autophagy by inducing rapid cell death.

Additionally, LC3 protein is known to exist in two cellular forms such as LC3-I and LC3-II. LC3-I is converted to LC3-II by conjugation to phosphatidylethanolamine, and the amount of LC3-II is a good early marker for the formation of autophagosomes.[36,37] During 96 hr exposure to VK2, we analyzed the amount of LC3-II and also assessed the cleaved forms of caspase-3 as marker for apoptosis in HL-60*neo*/*bcl-2* cells. In HL-60*neo* cells, the amount of LC3B-II increased within 48 hrs of exposure to VK2. In HL-60 *bcl-2* cells the amount of LC3B-II was detected after 72–96 hr exposure to VK2 (Fig. 3D). In addition, recent evidence suggests that the accumulation of LC3-II is more accurately represented in autophagic flux in the presence of lysosomal inhibitors.[38] In the presence of E-64-d and pepstatin A, endogenous LC3B-II increased after treatment with VK2 in both HL-60*neo* and HL-60*bcl-2* cells (Fig. 3E). Immunoblotting with anti-caspase-3 mAb revealed that the cleaved form of caspase-3 was significantly increased after treatment with VK2 for 48–96 hr in HL-60*neo* cells, whereas the cleaved caspase-3 was almost undetectable in HL-60*bcl-2* cells during the 96 hr-exposure to VK2 (Fig. 3D). These results demonstrated that both autophagy and apoptosis occurred at the same time in HL-60*neo* cells. In addition, autophagy was induced earlier in HL-60*neo* cells than in HL-60*bcl-2* cells during exposure to VK2. This was further confirmed by electron microscopy of HL-60*neo* cells without nuclear fragments but with chromatin condensation after treatment with VK2, which may represent the earlier phase of apoptosis. These cells showed autophagosomes and autolysosomes in the cytoplasm (Fig. 2A; lower). Interestingly, some HL-60*bcl-2* cells with chromatin condensation also showed autophagosome formation (Fig. 2B; lower).

All data shown above indicated that autophagy can be induced both in HL-60*neo* and HL-60*bcl-2* cells in response to VK2, but it becomes more prominent in HL-60*bcl-2* cells because the cells are protected from rapid apoptotic cell death after 96 hr-treatment with VK2. In addition, HL-60*neo* cells undergo both autophagy and apoptosis. To confirm this evidence, we further examined the effect of Z-DEVD-FMK, a caspase-3 inhibitor, in HL-60*neo* cells. HL-60*neo* cells were cultured with Z-DEVD-FMK at various concentrations with/without 10 μM VK2. As shown in Figure 4A, cell growth inhibition by VK2 was attenuated in the presence of 10 μM and 100 μM of Z-DEVD-FMK. Z-DEVD-FMK alone at these concentrations did not show any cytotoxic effect during 96 hr-exposure. Then, HL-60*neo* cells were treated with VK2 with/without 100 μM of Z-DEVD-FMK for the assessment of autophagy induction. Since many cells were lost via apoptosis during 96 hr-exposure to VK2 without Z-DEVD-FMK, cellular proteins were lysed and protein contents were equalized for immunoblottings. Z-DEVD-FMK showed significant inhibition of VK2-induced caspase-3 activation as assessed by capsease-3 cleavage. Notably, autophagy induction assessed by LC3B-II formation was significantly enhanced in the presence of Z-DEVD-FMK after 96 hr exposure to VK2 (Fig. 4B). These data also supported that autophagy becomes more prominent by blocking apoptotic cell death.

Mixed morphologic feature of autophagy and apoptosis in HL-60*bcl-2* cells. The data shown above led us to further examine the morphologic features of HL-60*bcl-2* and HL-60*neo* cells in detail after exposure to VK2.

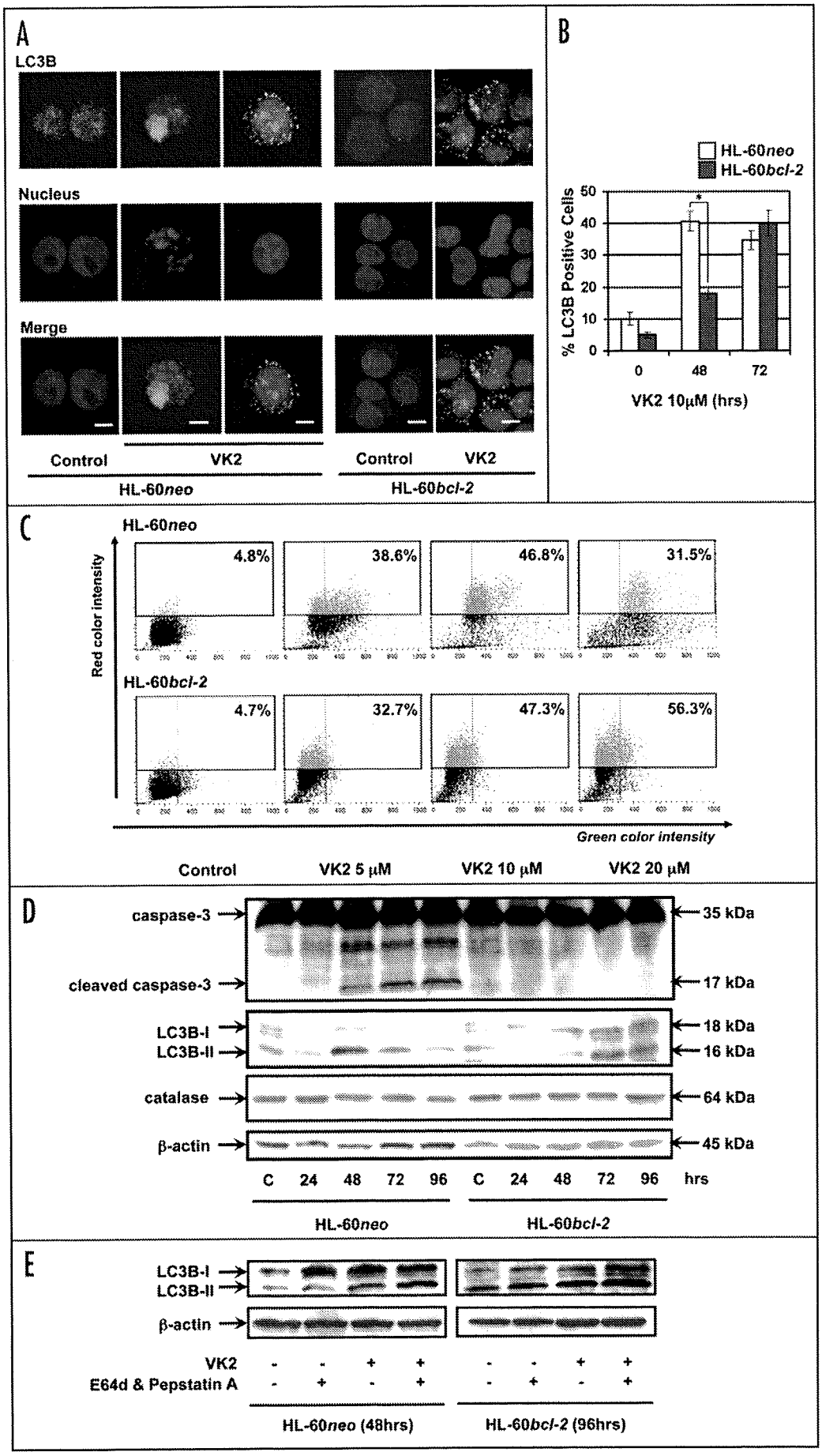

Figure 3. Induction of autophagy in response to VK2 in HL-60*neo*/HL-60*bcl-2* cells. *Involvement of LC3B in VK2-induced autophagy:* After exposure to 10 μM VK2 for 48 and 72 hr, the cells were processed for fluorescent immunocytostaining with anti-LC3B Ab and counterstaining with DAPI for nucleus as described in Materials ant Methods. (A) HL-60*neo*/*bcl-2* cells (original magnification x 1,000). (B) Quantification of the cells showing the punctuated pattern of LC3B staining, which marks cells with autophagosome formation. One hundred cells were assessed and ratios for the cells showing the punctuated pattern of LC3B staining were expressed. Results shown are the means ± SD from the results of three independent experiments. *$p < 0.001$. *Development of acidic vesicular organelles (AVOs) after VK2 treatment:* (C) After staining the cells with acridine orange, AVOs were quantified using flowcytometer in HL-60*neo* (upper) and HL-60*bcl-2* (lower) treated with or without VK2 (5 μM, 10 μM or 20 μM) for 72 hr. X-axis, green color intensity; Y-axis, red color intensity. *Expression of isoforms of LC3B and caspase-3:* (D) Cellular proteins were lysed at the indicated time after incubation with or without 10 μM of VK2. Proteins were separated by either 11.25% or 15% SDS-PAGE. Aliquots of 40 μg of protein extracts were used for immunoblotting using anti-caspase-3 and anti-LC3B Abs, respectively. The anti-β-actin mAb was used for protein-loading equivalence. *Expression of isoforms of LC3B in the presence and absence of protease inhibitors:* (E) After treatment with 10 μM of VK2 for 44 hrs in HL-60*neo* and for 92 hrs in HL-60*bcl-2* cells, cells were further cultured with/without protease inhibitors, E-64-d (10 μg/ml) and pepstatin A (10 μg/ml) in the presence of VK2 for 4 hrs. Cellular proteins were lysed and immunoblotted with anti-LC3B Ab.

After exposure to VK2 for 96 hr, HL-60*bcl-2* cells showed an increased percentage of fragmented nuclei compared to 72 hr treatment. Intriguingly, the morphologic findings in HL-60*bcl-2* cells undergoing apoptosis were different from those in HL-60*neo* cells; each nuclear fragment appeared to be encapsulated by vesicles resulting in the formation of a "sunny side-up" appearance (Fig. 5A). A "sunny side-up" appearance was also observed in HL-60*neo* cells treated with VK2 in the presence of a caspase-3 inhibitor, Z-DEVD-FMK. Extended exposure to VK2 up to 6 days resulted in the disappearance

of this characteristic feature and the appearance of the typical apoptotic bodies like in HL-60*neo* cells treated with 72 hr exposure to VK2 (Fig. 5B). Therefore, this morphologic change in HL-60*bcl-2* cells seems to be an early phase of cells undergoing apoptosis. To investigate whether the "sunny side-up" feature is macroautophagy of nuclear fragments, we examined the VK2 treated HL-60*bcl-2* cells by electron microscopy. Fragmented nuclei with condensed chromatin appeared to be surrounded by double-membrane (Fig. 5C). However, fluorescent immunocytostaining with anti-LC3B Ab showed that nuclear fragments were not surrounded by punctuated LC3B. Therefore, "sunny side-up" feature does not appear to represent the macroautophagy of nuclear fragments.

The biological roles of VK2-induced autophagy in HL-60*neo/bcl-2* cells. Since autophagy was initially recognized as a cellular survival process under amino acid starvation,[23,24] the concept of autophagic cell death as type II PCD and the significance of cancer treatment-induced autophagy is a subject of debate. Autophagy may function as an anti-cancer effect or a cytoprotective reaction against the cytotoxic reagents.[20-22] To assess the role of VK2-induced autophagy in HL-60 cells, we attempted to block the autophagic process in the presence or absence of VK2 using 3-MA, an inhibitor of class III phosophatidyl-inositol-3 kinase (PI3K),[31] and siRNA against Atg7, respectively. Treatment with 3-MA suppressed the PI-staining positive cells in HL-60*neo/bcl-2* cells treated with VK2. 3-MA alone showed no effect on HL-60 cell growth. In addition, the decreased viability of HL-60*neo* and HL-60*bcl-2* cells after VK2 treatment was reversed in the presence of 3-MA (Fig. 6A and B). Furthermore, 3-MA suppressed the induction of AVOs in HL-60*neo/bcl-2* cells treated with VK2 (Fig. 6C). siRNA effectively suppressed Atg7 expression in HL-60neo/*bcl-2* cells. Suppression of Atg7 resulted in significant attenuation of cell growth inhibition by VK2 in both cell lines (Fig. 6D). All these data support the conclusion that autophagic cell death was induced after treatment with VK2. To further confirm this interpretation, we used the Tet-off system with an Atg5$^{-/-}$ mouse embryonic fibroblast (MEF) cell line.[33] Pretreatment of Tet-off Atg5$^{-/-}$ MEF cells with 10 ng/ml doxycycline hydrochloride (Dox) for 120 hrs induced complete suppression of Atg5 expression. Thereafter, the cells were further cultured in the presence or absence of VK2 for 72 hrs. As shown in Figure 7, the VK2- induced cell growth inhibition at 10 μM was significantly attenuated in Dox treated-MEF cells along with suppression of the induction of LC3B-II. These data also support the occurrence of autophagic cell death in response to VK2.

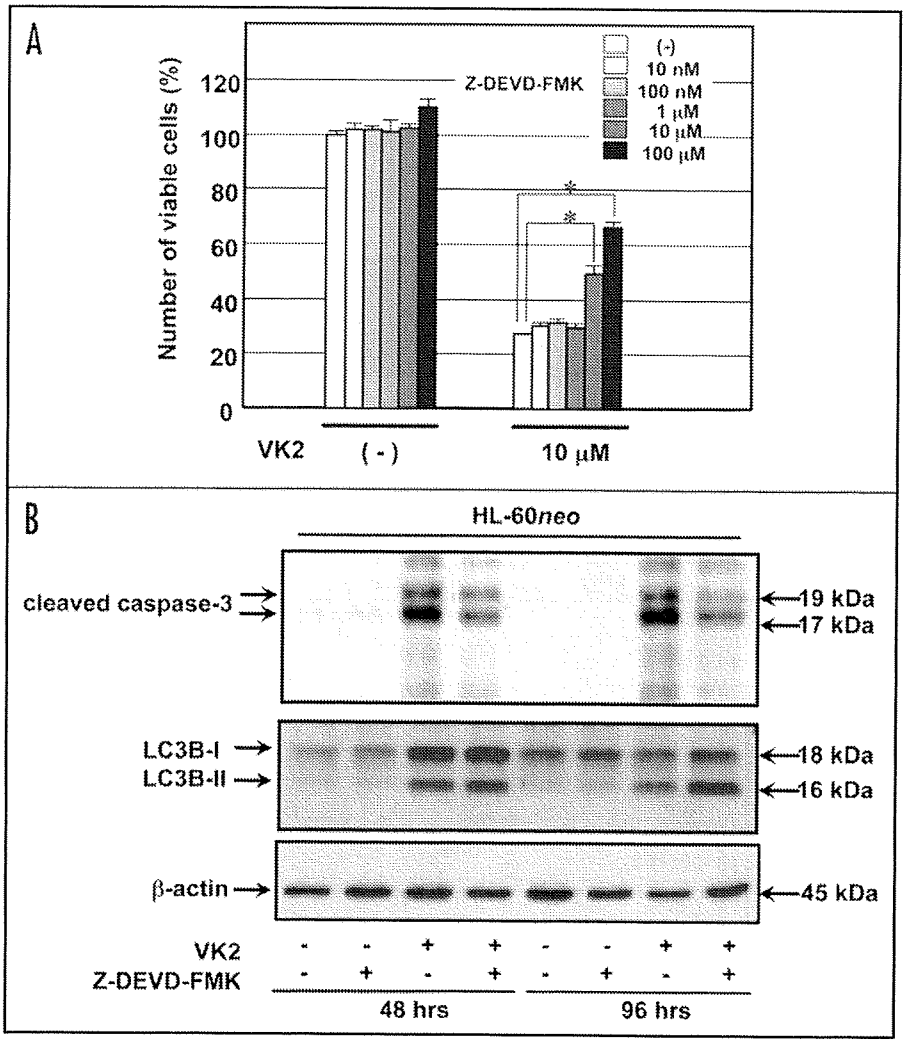

Figure 4. Effects of a caspase-3 inhibitor on VK2-induced autophagy in HL-60*neo* cells. (A) HL-60*neo* cells were cultured with Z-DEVD-FMK at various concentrations with/without 10 μM of VK2 for 96 hr. The number of cells was assessed with the WST cell counting kit as described in Materials and Methods. *$p < 0.001$. (B) HL-60*neo* cells were treated with 10 μM VK2 with/without 100 μM of Z-DEVD-FMK for 48 hr and 96 hr, respectively. Cellular proteins were lysed and separated by either 11.25% or 15% SDS-PAGE. Aliquots of 40 μg of protein extracts were used for immunoblotting using anti-cleaved caspase-3 Ab, anti-LC3B Ab, and anti-β-actin mAb, respectively.

Discussion

In the present study, we demonstrated that VK2 induces autophagy as well as apoptosis in HL-60 cells. In addition, the mixed morphologic features of apoptosis and autophagy such as chromatin condensation and fragmented nuclei for apoptosis and autophagosomes and autolysosomes for autophagy were detected in the same cells (Fig. 2A and B). This suggests that the cellular processes for apoptosis and autophagy are simultaneously induced in response to VK2 as well as some previous reports in Drosophila and sympathetic neurons.[39,40] Immunoblottings for LC3B and caspse-3, which were performed for assessment of autophagy and apoptosis induction, also support this evidence (Fig. 3D). During extended exposure to VK2 in cells with higher expression of Bcl-2, autophagy became more evident, because cells with lower expression of Bcl-2 underwent apoptotic cell death and were eliminated from culture system. This indicates that the cellular expression levels of Bcl-2 appear to determine the phenotype of cell death. Induction of autophagy in cancer cells in response to various anti-cancer reagents has been reported: Temozolomide (TMZ), a DNA alkylating agent, and arsenic trioxide

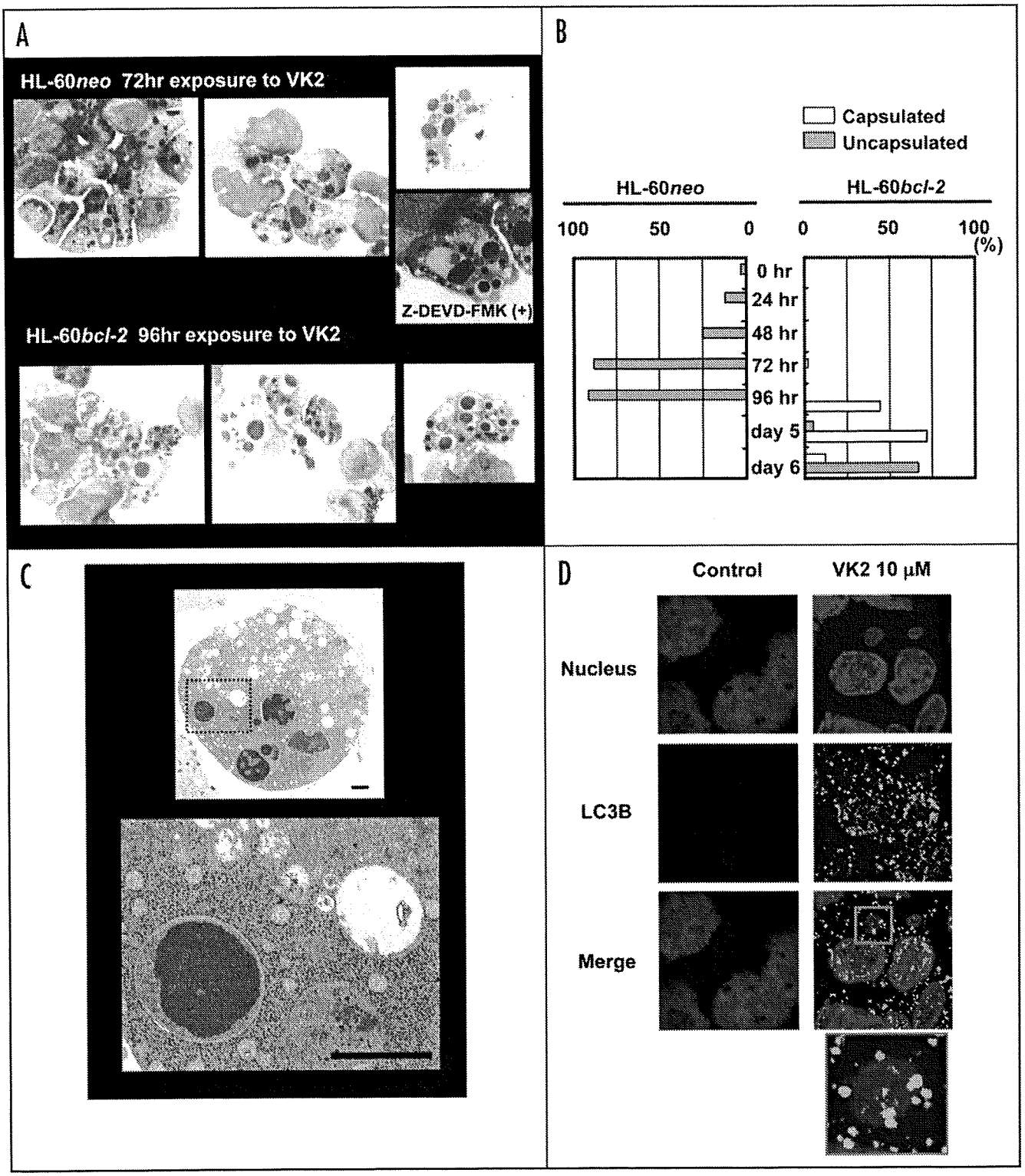

Figure 5. Capsulated fragmented nuclei in HL-60*bcl-2* cells after treatment with VK2. (A) Morphological features of HL-60*neo* after 72 hr-treatment with VK2 (10 μM) with/without Z-DEVD-FMK (100 μM) and of HL-60*bcl-2* cells after 96 hr-treatment with VK2. May-Grünwald-Giemsa staining, original magnification x 1,000. (B) Percentages of HL-60 cells with apoptotic bodies containing either capsulated nuclear fragments or uncapsulated nuclear. After treatment HL-60*neo/bcl-2* cells with 10 μM of VK2 for various length of time, morphologic changes were assessed in 100 cells after May-Grünwald Giemsa stain as well as Figure 4A. (This is one of representative result from 3 separate experiments.) (C) Electron microscopy of HL-60*bcl-2* cells after treatment with 10 μM VK2 for 96 hr. (D) Fluorescent immunocytostaining with anti-LC3B Ab in HL-60*bcl-2* cells after 96 hr-treatment with 10 μM VK2. Fluorescent immunocytostaining with anti-LC3B Ab (original magnification x 1,000) was performed as described in Figure 3A and C, respectively. The slides stained with anti-LC3B Ab were monitored using Zeiss LSM510 confocal microscope (Original magnification x 600).

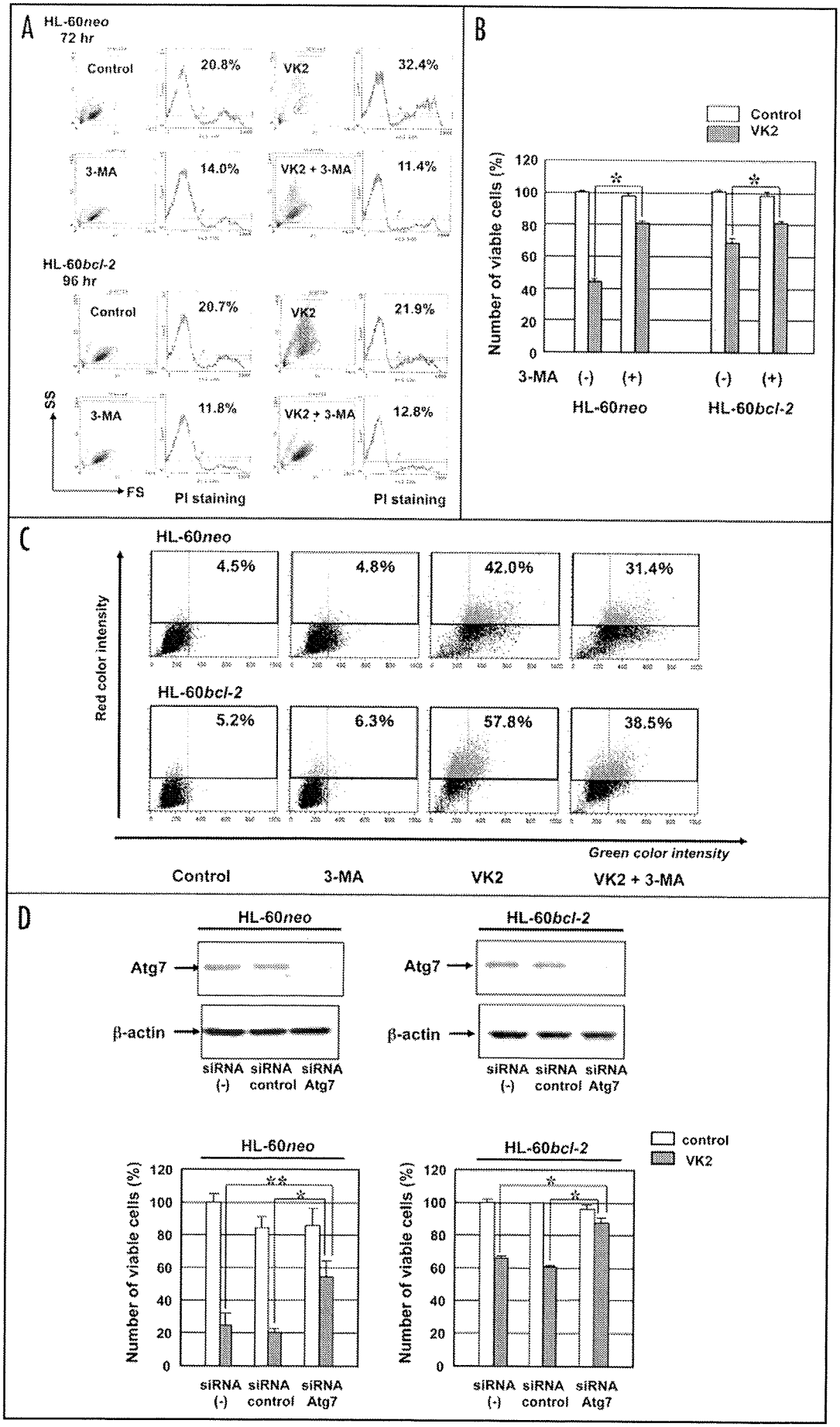

Figure 6. Effects of inhibition of VK2-induced autophagy in HL-60*neo*/*bcl-2* cells. (A and B) To inhibit autophagy, 2 mM 3-MA was added to HL-60 cell cultures for 72 hr with or without VK2. Viable cell numbers were assessed using a flow cytometer as described in Materials and Methods. *p < 0.001 (C) Treatment with 3-MA suppressed the induction of acidic vesicular organelles (AVOs) in HL-60*neo*/*bcl-2* cells treated with 10 μM of VK2. AVOs were quantified with fluorescence-activated cell sorter in HL-60*neo* (upper)/HL-60*bcl-2* (bottom). x-axis, green color intensity; y-axis, red color intensity. (D) Inhibition of Atg7 protein expression by siRNA transfection: HL-60neo/*bcl-2* cells were transfected with random siRNA or siRNA for Atg7 for 72 hrs. Relative expression levels of Atg7 proteins were assessed by western blotting. (upper). After treatment with/without random siRNA or siRNA for ATG7, the cells were further treated with VK2 for 72 hrs. Thereafter, cell growth inhibition was assessed by WST cell counting kit (lower). *p < 0.001, **p < 0.05.

(As_2O_3) induce autophagy of malignant glioma cells, which are usually refractory to various anti-cancer therapies.[30,41] The histone deacetylase inhibitors sodium butyrates and suberoylanilide hydeoxamic acid (SAHA) induce autophagic cell death in HeLa cells which overexpress the anti-apoptotic protein Bcl-X_L, but they induce apoptosis in parental HeLa cells.[42] Murine L929 fibroblastic cells, murine RAW 264.7 macrophages, and human U937 leukemia cells underwent autophagy after treatment with z-VAD-fmk, a pancaspase inhibitor.[43] Etoposide induces autophagic cell death in Bax/Bak-double knockout MEF, and these cells also undergo protective autophagy under conditions of nutrition depletion.[44] These conditions for induction of autophagy by cytotoxic stimuli include cellular resistance against apoptosis or protection from apoptosis. Our observations showing autophagy in HL-60*bcl-2* rather than HL-60*neo* cells meet these conditions. However, our data also demonstrated that apoptotic and

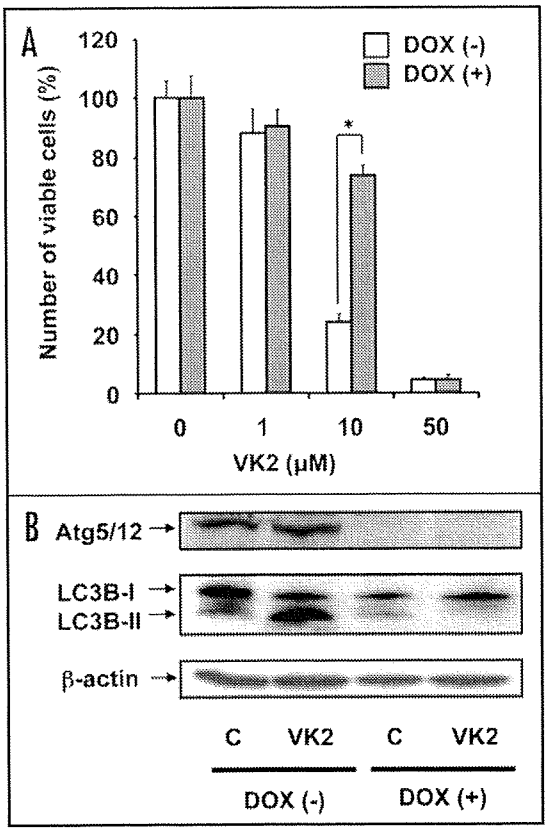

Figure 7. Effects of inhibition of VK2-inducing autophagy in a Atg5$^{-/-}$ mouse embryonic fibroblast (MEF) cell line with the Atg5 Tet-off system. Tet-off Atg5 MEF cells were incubated with 10 ng/ml doxycycline hydrochloride (Dox) for 120 hrs, and thereafter cultured in the presence or absence of 1 to 50 μM of VK2 for 72 hrs. (A) Cell growth inhibition in response to VK2 was assessed using WST assay kit. (B) MEF cells treated with or without Dox were cultured in the presence or absence of 10 μM of VK2 for 72 hr. Then, cellular proteins were separated by 11.25% SDS-PAGE and immunoblotted with either anti-Atg5, anti-LC3B, or anti-β-actin Abs.

autophagic processes can be simultaneously induced by VK2 (Figs. 2 and 3).[39,40] Therefore, cell death induced by cytotoxic reagents cannot be simply characterized in stereotyped manner such as type I PCD versus type II PCD.

Although autophagy became evident in HL-60*bcl-2* cells, previous reports have demonstrated that Bcl-2 negatively regulates induction of autophagy. Bcl-2 localized on endoplasmic reticulum was reported to interact with Beclin 1 and to inhibit Beclin 1-dependent autophagy.[27] This anti-autophagy function of Bcl-2 was suggested to help maintain autophagy at the levels that are compatible with cell survival, rather than cell death.[27] In addition, downregulation of Bcl-2 by the conditional expression of the full length bcl-2 antisense message was reported to induce autophagic cell death in HL-60 cells,[26] and Bcl-2/Bcl-X_L antagonist HA14-1 also induces autophagy and apoptosis in L1210 murine leukemia cells,[45] suggesting anti-autophagic function of Bcl-2. In our data, comparing autophagy induction between HL-60*neo* and HL-60*bcl-2* by the formation of punctuated LC3B, autophagy was rather enhanced in HL-60*neo* cells within 72 hrs of exposure to VK2 (Fig. 3B). Delayed induction of autophagy in HL-60*bcl-2* as assessed by conversion of LC3B type I to type II was also observed (Fig. 3D). These data agree with previous reports that Bcl-2 has a negative effect on the induction of autophagy. However, since *bcl-2* knockout mice are viable with almost intact bone marrow functions,[46] other regulatory pathway(s) might be involved for autophagy, especially when the cells are exposed to cytotoxic reagents. It has been reported that intracellular calcium mediates the induction of autophagy in a Bcl-2 regulated fashion.[47] These findings raise the question as to how a cell decides to undergo either apoptosis or autophagy in response to calcium signals.

It was intriguing that some morphologic features of the same death pathway differed between HL-60*neo* and HL-60*bcl-2* cells. As shown in Figure 5A and B, nuclear fragments were capsulated in HL-60*bcl-2* cells but not in HL60*neo* cells. Longer exposure to VK2 resulted in disappearance of this "sunny side-up" feature which seems to detect an early phase of apoptosis. These encapsulated nuclear fragments should be designated as "apoptotic bodies" as in previous reports.[48] The formation of "sunny side-up" may be only detectable under conditions for autophagy inductions along with a higher threshold for apoptosis such as overexpression of anti-apoptotic Bcl-2 proteins or in the presence of a caspase-3 inhibitor. However, we could not prove the macroautophagy formation of fragmented nuclei by LC3B fluorescence immunocytostaining (Fig. 5D) Biological significance of this distinct phenomenon remains to be cleared.

Although "autophagic cell death" has recently been clearly demonstrated in salivary gland cells during development of Drosophila,[49] the concept of autophagy as type II PCD is still controversial, especially the cell death induced by anti-cancer reagents.[20-22] In the presence of 3-MA, an inhibitor of type III PI3K, VK2-induced cell death was significantly suppressed not only in HL-60*bcl-2* but also in HL-60*neo* cells (Fig. 6A–C). This suggests that the VK2-induced autophagy induces cell death. However, 3-MA is not a specific inhibitor for autophagy and it may interact with other signaling pathways for cell death.[22,37] Knockdown of Atg7 with siRNA prevented VK2-induced cell death (Fig. 6D). Tet-off Atg5 MEF system also demonstrated an attenuation of VK2-induced cell growth inhibition along with inhibition of autophagy (Fig. 7). Therefore, the enhanced autophagy in response to VK2 is correlated with induction for cell death in our system. These lines of evidence strongly suggest "autophagic cell death" or "autophagy medicated cell death" in leukemia cells. However, the executor(s) for induction of cell death still remains to be cleared. Yu Li et al., reported that caspase inhibition leading to cell death by means of autophagy involves accumulation of reactive oxygen species (ROS), membrane lipid oxidation, and loss of plasma membrane integrity in L929 cells.[50] The accumulation of abnormal ROS was caused by the selective autophagic degradation of the catalase, which is the major enzymatic ROS scavenger.[50] The accumulation of ROS following degradation of catalase might be one of the executors of autophagic cell death when caspases are inhibited. However, as shown in Figures 1A and 3D, catalase expression was not different between HL-60*neo* and HL-60*bcl-2* cells, and no significant change of catalase expression during 96 hr exposure to VK2. Therefore, our observation cannot be explained by degradation of catalase. In fat body cells and wing discs of Drosophila, overexpression of Atg1 itself was sufficient to induce autophagy along with apoptosis in a caspase-dependent manner.[40] This suggests that autophagy represents an alternative induction of apoptosis rather than a distinct form of cell death. In contrast, autophagy is activated by apoptotic signaling in sympathetic neurons.[39] In this system, the same apoptotic signal induces

mitochondrial dysfunction and also activates autophagy. Once it was activated, autophagy was suggested to mediate caspase-independent neuronal death.[39] It is noteworthy that knockdown of Atg7 using siRNA as well as 3-MA treatment showed attenuation of growth inhibition by VK2 in HL-60*neo* cells (Fig. 6D). Since apoptotic cell death should be dominant in HL-60*neo* cells, autophagy may function as an alternative inducer for apoptosis. This may be further supported by the distinct morphologic change in some but not all HL-60*bcl-2* cells after longer exposure to VK2, which showed apoptotic bodies with "sunny side-up" feature (Fig. 4A and B).

Qu X et al., demonstrated that autophagy contributes to the clearance of dead cell by a mechanism that likely involves the generation of energy-dependent engulfment signals.[51] This suggests an extended role for autophagy in the disposal of dead cells by a phagocytic system in vivo. Although this novel function of autophagy for PCD was demonstrated in ES cells during embryonic development, it may also extend to cancer cells. Autophagy induction in response to VK2 may explain the selective clearance of a leukemic clone via the phagocytic system in vivo.[2,6,11] Autophagy induction by VK2 shown in this study may give us novel therapeutic tools in the treatment of leukemia.

Materials and Methods

Cell lines and reagents. HL-60 cells obtained from the American Type Culture Collection (Rockville, MD) were maintained in continuous culture in RPMI 1640 medium (GIBCO, Grand Island, NY) supplemented with 10% FCS (Hyclone, Logan, UT), 2 mM L-glutamine, penicillin (50 U/ml), and streptomycin (100 μg/ml). A clone stably transfected with the human *bcl-2* gene, HL-60*bcl-2*, was established by electroporation using a recombinant pdDNA3-plasmid-containing the human *bcl-2a* gene.[26] HL-60*neo* is a control cell line transfected with pdDNA3-plasmid alone.[26] VK2 (menaquinon-4) was supplied by Eisai Co., Ltd. (Tokyo, Japan). E-64-d and Pepstatin A, which are inhibitors for lysosomal proteases, were purchased from BIOMOL International L.P. (Plymouth Meeting, PA). Z-DEVD-FMK for a caspase-3 inhibitor was purchased from R & D Systems Inc. (Minneapolis, MN).

Assessment of viable cell count. HL-60 cells treated with or without VK2 were stained with a solution containing 1% (v/v) propidium iodide (PI) (Sigma-Aldrich, St. Louis, MO) for 30 min at 4°C. First, the gating area of cytogram for detecting viable HL-60 cells was established according to both the PI staining-negative area (indicating viable cells) and the forward- and side- scatter intensities.[2] Then the cell cultures were pipetted gently to obtain uniform cell suspension, and were introduced to a flow cytometer. The number of cells in gating area for viable HL-60 cells was assessed for 60 sec. The number relative to the cells treated with control medium revealed to be well-correlated with the results obtained from a WST Cell Counting Kit (Dojin East, Tokyo, Japan), with absorption measurements at 450 nm.[2] In some experiments viable cell counts were assessed by trypan blue dye exclusion.

Quantitative detection of acid vesicular organelles (AVOs) with acridine orange staining. Autophagy is the process of sequestrating cytoplasmic proteins and organelles into the lysosomal component and characterized by development of AVOs. To detect and quantify AVOs in VK2-treated cells, we performed vital staining with acridine orange (Polysciences, Warrington, PA) as described previously.[29,30] To inhibit autophagy 2 mM 3-methyladenine (3-MA) (Polysciences Inc, Warrington, PA), an inhibitor of the phosphatidylinositol 3-kinase (PI3K),[31] was added to the cultures for 72 hr with/without VK2. HL-60 cells were stained with 1.0 μg/ml acridine orange for 15 min at room temperature and processed for flow cytometry using the FACScan Cytometer (Becton Dickinson, San Jose, CA) and analyzed with CellQuest software (Becton Dickinson).

Immunoblotting. Cells were lysed in Lysis Buffer (10 mM Tris-HCL PH 7.8, 150 mM NaCl, 1% NP-40, 1 mM EDTA, 10% glycerol, 1 mM phenylmethylsulfonyl fluoride, 0.15 U/ml aportinine, 10 mg/ml leupeptine, 100 mM sodium fluoride, 2 mM sodium orthovanadate), and cellular proteins were quantified using the Protein Assay kit of Bio-Rad (Richmond, CA). Equal amounts of proteins were loaded, separated by SDS-PAGE and transferred onto Hybond-P membranes (Amersham Biosciences Corp., Piscataway, NJ). The membranes were probed with antibodies (Abs) such as anti-human Bcl-2 monoclonal (m) Ab (BD Biosciences Pharmingen, San Jose, CA), anti-microtubule-associated protein 1 light chain 3B (LC3B) Ab, anti-caspase-3 Ab (Cell Signaling Technology, Danvers, MA), anti-cleaved caspase-3 Ab (Cell Signaling Technology), anti-Atg5 Ab (Abgent, San Diego, CA), anti-Atg7 Ab (ProSci, Poway, CA), anti-human catalase rabbit mAb (Epitomics Inc., Burlingame, CA), and anti-β-actin Ab (Sigma-Aldrich), respectively. Anti-LC3B Ab was generated as previously described.[32] Immunoreactive proteins were detected by horseradish peroxidase-conjugated second Ab and an enhanced chemiluminescence reagent (ECL) (Amersham Biosciences Corp.).[3]

Assessment of apoptosis. Apoptosis was detected by morphology, flow cytometry using Annexin V-florescein isothiocyanate (FITC) apoptosis detection kit I (BD Biosciences, San Diego, CA), and by immunoblotting with either anti-caspase-3 or anti-cleaved caspase-3 Abs as described above. For flow cytometry, HL-60 cells treated with or without VK2 were washed twice with ice cold phosphate-buffered saline and then resuspended in 1 X binding buffer (1 x 10^6 cells/ml). 100 μl of cell suspension (1 x 10^5 cells) was then transferred to a 5 ml tube, and 5 μl of Annexin V-PE and 5 μl of 7-amino-actinomycin were added. After 15 min of incubation at room temperature in the dark, 400 μl of 1 X binding buffer was added and the tubes were analyzed in a FACScan instrument with CellQuest software (Becton Dickinson). For morphologic assessment for apoptosis, the cell suspension was sedimented in a Shandon Cytospin II (Shandon, Pittsburgh, PA), and preparations were stained with May-Grünwald-Giemsa and with 4'-6-diamidino-2-phenylindole (DAPI, Vector laboratories, Inc., Burlingame, CA).

Measurement of mitochondrial membrane potential. Mitochondrial membrane potential was measured with tetramethyl rhodamine ethyl ester perchlorate (TMRE: Molecular Probe Inc., Eugene, OR) using flow cytometry as described previously.[30] Cells were incubated with 150 nM TMRE at 37°C for 20 min in the dark and analyzed by FACScan using CellQuest software. The fluorescent dye TMRE is accumulated by mitochondria as a result of the mitochondrial membrane potential. Shift to the left in the emission spectrum indicates the depolarization of mitochondrial membrane potential in the apoptotic cells.

Electron microscopy. HL-60 cells were treated with/without VK2 and then fixed with a solution containing 3% glutaraldehyde plus 2% paraformaldehyde in 0.1 M cacodylate buffer (pH 7.3) for

1 hr. The samples were further post-fixed in 1% OsO_4 in the same buffer for 1 hr, and subject to the electron microscopic analysis using an electron microscope H-7000 (Hitachi, Tokyo, Japan) as described previously.[30] Representative areas were chosen for ultra-thin sectioning and viewed with an electron microscope.

Fluorescent immunocytostaining. Cells were fixed on glass slide by Shandon Cytospin II followed by further fixation with 4% paraformaldehyde for 20 min. After fixation, the cells on the slides were incubated with anti-LC3B Ab (1:5,000 dilution) in 0.5% Triton X-100-phosphate-buffered saline (PBS) overnight at 4°C. The slides were then washed with PBS and incubated with Alexa Fluor 488-labeled secondary goat anti-rabbit Ab (1:200 dilution) for 1 hr at room temperature. The slides were mounted with DAPI and monitored under an Axioskop 40 (Carl Zeiss MicroImaging, Inc., Thornwood, NY) or LSM 510 (Carl Zeiss MicroImaging).

Small interfering RNA (siRNA) experiments. siRNA oligonucleotides for human Atg7 (accession # NM-006395, catalog # L-020112), and siCONTROL non-targeting siRNA (catalog # D-001220) were purchased from GE Healthcare UK Ltd. (Buckinghamshire, England), and resuspended in RNase-free H_2O at 20 μM. HL-60*bcl-2* cells were washed twice in serum-free media and resuspended to 1 x 10^7 cells per 500 μl of cold, serum-free OPTI-MEM (GIBCO), and transferred to pre-chilled 0.4 cm-gap electroporation curettes (Bio-Rad). Cells were mixed with/without siRNA at 20 nM (final concentration) on ice for 5 min, thereafter, cells were pulsed once at 250 mV, 960 μF by using a Bio-Rad electroporator. The cell suspensions were then transferred to the incubator in 5% CO_2 at 37°C. Five hr after electroporation, the same volume of RPMI 1640 medium containing 20% FBS was added. Forty-eight hr after electroporation, protein knockdown was determined by immunoblotting, and the cells were treated with the indicated concentration of VK2 for 72 to 96 hr, and viable cells were assessed as previously described.

Tet-off system with an Atg5$^{-/-}$ mouse embryonic fibroblasts (MEFs). The Atg5 Tet-off MEF cell line was a kind gift from Dr Noboru Mizushima (Tokyo Medical and Dental University School of Health Science, Tokyo, Japan).[33] Atg 5 expression can be completely suppressed when this cell line is cultured in the presence of doxycycline. The culture condition is precisely described in elsewhere.[33]

Statistics. All data are given as the mean ± SD. Statistical analysis was performed by using Mann-Whitney's U test (two-tailed). The criterion for statistical significance was taken as $p < 0.05$.

Acknowledgements

We thank Ayako Hirota and Fumiko Komoda for their excellent technical assistance and Dr. Noboru Mizushima of Tokyo Medical and Dental University School of Health Science for a kind gift of the Atg5 Tet-off MEF cell line. We also thank Eisai Co. for providing menaquinone-4.

This study is supported by a Grant-in-Aid for Science Research (C) from the Ministry for Education, Science, Sports and Culture of Japan to K.M. (#18591089).

References

1. Lamson DW, Plaza SM. The anticancer effects of vitamin K. Altern Med Rev 2003; 8:303-18.
2. Yaguchi M, Miyazawa K, Katagiri T, Nishimaki J. Kizaki M, Tohyama K, Toyama K. Vitamin K2 and its derivatives induce apoptosis in leukemia cells and enhance of all-*trans* retinoic acid. Leukemia 1997; 11:779-87.
3. Yokoyama T, Miyazawa K, Yoshida T, Ohyashiki K. Combination of vitamin K2 plus imatinib mesylate enhances induction of apoptosis in small cell lung cancer cell lines. Int J Oncol 2005; 26:33-40.
4. Wang Z, Wang M, Finn F, Carr BI. The growth inhibitory effects of vitamins K and their actions on gene expression. Heparology 1995; 22:876-82.
5. Otsuka M, Kato N, Shao RX, Hoshida Y, Ijichi H, Koike Y, Taniguchi H, Moriyama M, Shiratori Y, Kawabe T, Omata M. Vitamin K2 inhibits the growth and invasiveness of hepatocellular carcinoma cells via protein kinase A activation. Hepatology 2004; 40:243-51.
6. Miyazawa K, Aizawa S. Vitamin K2 improves the hematopoietic supportive functions of bone marrow stromal cells in vitro: a possible mechanism of improvement of cytopenia for refractory anemia in response to vitamin K2 therapy. Stem Cells Dev 2004; 5:449-51.
7. Miyazawa K, Nishimaki J, Ohyashiki K, Enomoto S, Kuriya S, Fukuda R, Hotta T, Teramura M, Mizoguchi H, Uchiyama T, Omine M. Vitamin K2 therapy for myelodysplastic syndrome (MDS) and post-MDS acute myeloid leukemia: Information through a questionnaire survey of multi-center pilot studies in Japan. Leukemia 2000; 14:1156-7.
8. Yaguchi M, Miyazawa K, Otawa M, Ito Y, Kawanishi Y, Toyama K. Vitamin K2 therapy for a patient with myelodysplastic syndrome. Leukemia 1999; 13:144-5.
9. Habu D, Shiomi S, Tamori A, Takeda T, Tanaka T, Kubo S, Nishiguchi S. Role of vitamin K_2 in the development of hepatocellular carcinoma in women with viral cirrhosis of the liver. *JAMA* 2004; 292:358-61.
10. Mizuta T, Ozaki I, Eguchi Y, Yasutake T, Kawazoe S, Fujimoto K, Yamamoto K. The effect of menatetrenone, a vitamin K_2 analog, on disease recurrence and survival in patients with hepatocellular carcinoma after curative treatment: a pilot study. Cancer 2006; 106:867-72.
11. Yaguchi M, Miyazawa K, Otawa M, Katagiri T, Nishimaki J, Uchida Y, Iwase O, Gotoh A, Kawanishi Y, Toyama K. Vitamin K2 selectively induces apoptosis of blastic cells in myelodysplastic syndrome: Flow cytometric detection of apoptotic cells using APO2.7 monoclonal antibody. Leukemia 1998; 12:1392-7.
12. Miyazawa K, Yaguchi M, Funato K, Gotoh A, Kawanishi Y, Nishizawa Y, Yuo A, Ohyashiki K. Apoptosis/differentiation-inducing effects of vitamin K2 on HL-60 cells: dichotomous nature of vitamin K2 in leukemia cells. Leukemia 2001; 15:1111-7.
13. Nishimaki J, Miyazawa K, Yaguchi M, Katagiri T, Kawanishi Y, Toyama K, Ohyashiki K, Hashimoto S, Nakaya K, Takiguchi T. Vitamin K2 induces apoptosis of a novel cell line established from a patient with myelodysplastic syndrome in blastic transformation. Leukemia 1999; 9:1399-405.
14. Matsumoto K, Okano J, Nagahara T, Murawaki Y. Apoptosis of liver cancer cells by vitamin K2 and enhancement by MEK inhibition. Int J Oncol 2006; 29:1501-8.
15. Kanamori T, Shimizu M, Okuno M, Matsushima-Nishiwaki R, Tsurumi H, Kojima S, Moriwaki H. Synergistic growth inhibition by acyclic retinoid and vitamin K2 in human hepatocellular carcinoma cells. Cancer Sci 2007; 98:431-7.
16. Martelli AM, Zweyer M, Ochs RL, Tazzari PL, Tabellini G, Narducci P, Bortul R. Nuclear apoptotic changes: an overview. J Cell Biochem 2001; 82:634-46.
17. Green DR, Reed JC. Mitochondria and apoptosis. Science 1998; 281:1309-12.
18. Reed JC. Apoptosis-targeted therapies for cancer. Cancer Cell 2003; 3:17-22.
19. Clarke P. Developmental cell death: morphological diversity and multiple mechanisms. Anat Embryol (Berl) 1990; 181:195-213.
20. Bursch W, Ellinger A, Gerner C, Frohwein U, Schulte-Hermann R. Programmed cell death (PCD). Apoptosis, autophagic PCD, or others? Ann N Y Acad Sci 2000; 926:1-12.
21. Kondo Y, Kanzawa T, Sawaya R, Kondo S. Role of autophagy in cancer development and response to therapy. Nat Rev Cancer 2005; 5:726-34.
22. Levine B, Yuan J. Autophagy in cell death: an innocent convict? J Clin Invest 2005; 115:2679-88.
23. Klionsky D J, Emr SD. Autophagy as a regulated pathway of cellular degradation. Science 2000; 290:1717-21.
24. Yoshimori T. Autophagy: a regulated bulk degradation process inside cells. Biochem Biophysical Research Communications 2004; 313:453-8.
25. Ohsumi Y. Molecular dissection of autophagy: two ubiquitin-like systems. Nat Rev Mol Cell Biol 2001; 3:211-6.
26. Saeki K, Yuo A, Okuma E, Yazaki Y, Susin SA, Kroemer G, Takaku F. Bcl-2 downregulation causes autophagy in a caspase-independent manner in human leukemic HL60 cells. Cell Death Differ 2000; 12:1263-9.
27. Pattingre S, Tassa A, Qu X, Garuti R, Liang XH, Mizushima N, Packer M, Schneider MD, Levine B. Bcl-2 antiapoptotic proteins inhibit Beclin 1-dependent autophagy. Cell 2005; 122:927-39.
28. Pattingre S, Levine B. Bcl-2 inhibition of autophagy: A new route to cancer? Cancer Res 2006; 66:2885-8.
29. Paglin S, Hollister T, Delohery T, Hackett N, McMahill M, Sphicas E, Domingo D, Yahalom J. A novel response of cancer cells to radiation involves autophagy and formation of acidic vesicles. Cancer Res 2001; 61:439-44.
30. Kanzawa T, Kondo Y, Ito H, Kondo S, Germano I. Induction of autophagic cell death in malignant glioma cells by arsenic trioxide. Cancer Res 2003; 63:2103-8.
31. Seglen PO, Gordon PB. 3-Methyladenine: specific inhibitor of autophagic/lysosomal protein degradation in isolated rat hepatocytes. Proc Natl Acad Sci USA 1982; 79:1889-92.
32. Aoki H, Takada Y, Kondo S, Sawaya R, Aggarwal BB, Kondo Y. Evidence that curcumin suppresses the growth of malignant gliomas in vitro and in vivo through induction of autophagy: role of Akt and extracellular signal-regulated kinase signaling pathways. Mol Pharmacol 2007; 72:29-39.
33. Hosokawa N, Hara Y, Mizushima N. Genaration of cell lines with teracycline-regulated autophagy and a role for autophagy in controlling cell size. FEBS Letters 2006; 580:2623-9.

34. Kabeya Y, Mizushima N, Ueno T, Yamamoto A, Kirisako T, Noda T, Kominami E, Ohsumi Y, Yoshimori T. LC3, a mammalian homologue of yeast Apg8p, is localized in autophagosome membranes after processing. EMBO J 2000; 19:5720-8.
35. Mizushima N. Methods for monitoring autophagy. Int J Biochem Cell Biol 2004; 36:2491-502.
36. Mizushima N, Yoshimori T. How to interpret LC3 immunoblotting. Autophagy 2007; 3:1-4.
37. Klionsky DJ, Abeliovich H, Agostinis P, et al. Guidelines for the use and interpretation of assays for monitoring autophagy in higher eukaryotes. Autophagy 2008; 4:151-75.
38. Tanida I, Minematsu-Ikeguchi N, Ueno T, Kominami E. Lysosomal turnover, but not a cellular level, of endogenous LC3 is a marker for autophagy. Autophagy 2005; 1:84-91.
39. Xue L, Fletcher GC, Tolkovsky AM. Autophagy is activated by apoptotic signalling in sympathetic neurons: an alternative mechanism of death execution. Mol Cell Neurosci 1999; 14:180-98.
40. Scott RC, Juhász G, Neufeld TP. Direct induction of autophagy by Atg1 inhibits cell growth and induces apoptotic cell death. Curr Biol 2007; 17:1-11.
41. Kanzawa T, Germano IM, Komata T, Ito H, Kondo Y, Kondo S. Role of autophagy in temozolomide-induced cytotoxicity for malignant glioma cells. Cell Death Differ 2004; 11:448-57.
42. Shao Y, Gao Z, Marks PA, Jiang X. Apoptotic and autophagic cell death induced by histone deacetylase inhibitors. Proc Natl Acad Sci USA 2004; 101:18030-5.
43. Yu L, Alva A, Su H, Dutt P, Freundt E, Welsh S, Baehrecke EH, Lenardo MJ. Regulation of an ATG7-beclin 1 program of autophagic cell death by caspase-8. Science 2004; 304:1500-2.
44. Shimizu S, Kanaseki T, Mizushima N, Mizuta T, Arakawa-Kobayashi S, Thompson CB, Tsujimoto Y. Role of Bcl-2 family proteins in a non-apoptotic programmed cell death dependent on autophagy genes. Nat Cell Biol 2004; 6:1221-8.
45. Kessel D, Reiners JJ Jr. Initiation of apoptosis and autophagy by the Bcl-2 antagonist HA14-1. Cancer Lett 2007; 249:294-9.
46. Nakayama K, Nakayama K, Negishi I, Kuida K, Sawa H, Loh DY. Targeted disruption of Bcl-2 alpha beta in mice: occurrence of gray hair, polycystic kidney disease, and lymphocytopenia. Proc Natl Acad Sci USA 1994; 91:3700-4.
47. Hoyer-Hansen M, Bastholm L, Szyniarowski P, Campanella M, Szabadkai G, Farkas T, Bianchi K, Fehrenbacher N, Elling F, Rizzuto R, Mathiasen IS, Jaattela M. Control of macroautophagy by calcium, calmodulin-dependent kinase kinase-beta, and Bcl-2. Mol Cell 2007; 25:193-205.
48. Martelli AM, Zweyer M, Ochs RL. Nuclear apoptotic changes: an overview. J Cellular Biochemistry 2001; 82:634-46.
49. Berry DL, Baehrecke EH. Growth arrest and autophagy are required for salivary gland cell degradation in Drosophila Cell 131:1137-48.
50. Yu L, Wan F, Dutta S, Welsh S, Liu Z, Freundt E, Baehrecke EH, Lenardo M. Autophagic programmed cell death by selective catalase degradation. Proc Natl Acad Sci USA 2006; 103:4952-7.
51. Qu X, Zou Z, Sun Q, Luby-Phelps K, Cheng P, Hogan RN, Gilpin C, Levine B. Autophagy gene-dependent clearance of apoptotic cells during embryonic development. Cell 2007; 128:931-46.

Down-regulation of TCF8 is involved in the leukemogenesis of adult T-cell leukemia/lymphoma

*Tomonori Hidaka,[1,2] *Shingo Nakahata,[1] *Kinta Hatakeyama,[3] Makoto Hamasaki,[1,4] Kiyoshi Yamashita,[2] Takashi Kohno,[5] Yasuhito Arai,[6] Tomohiko Taki,[7] Kazuhiro Nishida,[7] Akihiko Okayama,[8] Yujiro Asada,[3] Ryoji Yamaguchi,[9] Hirohito Tsubouchi,[2,10] Jun Yokota,[5] Masafumi Taniwaki,[7] Yujiro Higashi,[11] and Kazuhiro Morishita[1]

[1]Division of Tumor and Cellular Biochemistry, Department of Medical Sciences, [2]Department of Internal Medicine II, University of Miyazaki, Miyazaki; [3]First Department of Pathology, Faculty of Medicine, University of Miyazaki, Miyazaki; [4]Miyazaki Prefectural Industrial Foundation, Miyazaki; [5]Biology Division, National Cancer Center Research Institute, Tokyo; [6]Cancer Genome Project, National Cancer Center Research Institute, Tokyo; [7]Department of Hematology and Oncology, Kyoto Prefectural University of Medicine, Kyoto; [8]Department of Rheumatology, Infectious Diseases and Laboratory Medicine, University of Miyazaki, Miyazaki; [9]Department of Veterinary Pathology, University of Miyazaki, Miyazaki; [10]Department of Digestive and Life-style related Disease, Kagoshima University Graduate School of Medicine and Dental Sciences, Kagoshima; and [11]Graduate School of Frontier Biosciences, Osaka University, Osaka, Japan

Adult T-cell leukemia/lymphoma (ATLL) is caused by latent human T-lymphotropic virus-1 (HTLV-1) infection. To clarify the molecular mechanism underlying leukemogenesis after viral infection, we precisely mapped 605 chromosomal breakpoints in 61 ATLL cases by spectral karyotyping and identified frequent chromosomal breakpoints in 10p11, 14q11, and 14q32. Single nucleotide polymorphism (SNP) array–comparative genomic hybridization (CGH), genetic, and expression analyses of the genes mapped within a common breakpoint cluster region in 10p11.2 revealed that in ATLL cells, transcription factor 8 *(TCF8)* was frequently disrupted by several mechanisms, including mainly epigenetic dysregulation. *TCF8* mutant mice frequently developed invasive CD4+ T-cell lymphomas in the thymus or in ascitic fluid in vivo. Down-regulation of TCF8 expression in ATLL cells in vitro was associated with resistance to transforming growth factor β1 (TGF-β1), a well-known characteristic of ATLL cells, suggesting that escape from TGF-β1–mediated growth inhibition is important in the pathogenesis of ATLL. These findings indicate that *TCF8* has a tumor suppressor role in ATLL. (Blood. 2008;112:383-393)

Introduction

Adult T-cell leukemia/lymphoma (ATLL) is a peripheral CD4+ T-cell malignancy caused by infection with human T-lymphotropic virus-1 (HTLV-1).[1] HTLV-1 infection is endemic in a number of well-defined geographic regions within Japan, and as many as 20 million individuals worldwide are estimated to harbor it.[2] ATLL occurs after a prolonged latency period of up to 50 years in approximately 5% of individuals who have been infected with HTLV-1 around the time of birth. HTLV-1 encodes a transactivator, *Tax,* which plays a key role in the polyclonal growth of infected T cells through the activation of various genes.[3] However, recent studies have shown that Tax expression is undetectable in circulating ATLL cells, while a genetically and epigenetically defective provirus was observed in more than half of the ATLL patients examined.[4,5] Considering the long latency period of ATLL, it has been proposed that at least 5 additional genetic or epigenetic events are required for the development of overt disease.[1,6]

Nonrandom chromosomal translocations are considered to cause leukemic transformation, including structural and/or quantitative abnormalities of transcription factors such as *AML1, EVI1,* and *MLL.*[7] To identify disease-specific chromosomal translocations in ATLL, karyotypes of 107 ATLL cases determined by the G-banding method were reviewed in Japan.[8] There was a high degree of diversity and complexity, and disease-specific translocations were not found; however, translocations involving 14q32 (28%) or 14q11 (14%) and the deletion of 6q (23%) were the most frequent chromosomal abnormalities.[8] Recently, chromosome-based comparative genomic hybridization (CGH)[9] and BAC array-based CGH showed complex chromosomal abnormalities with gains in 1q, 2p, 4q, 7p, and 7q, and losses in 10p, 13q, 16q, and 18p.[10] To date, however, no gene involved in the development of ATLL has been isolated. Array CGH is useful for detecting genomic deletions or amplifications, but it cannot detect chromosomal translocations or inversions.

In this study, we searched for the existence of recurrent chromosomal rearrangements by multicolor spectral karyotyping (SKY) and high-resolution single nucleotide polymorphism (SNP) array-CGH (SNP array-CGH). We precisely mapped 605 chromosomal breakpoints in 61 ATLL cases. Breakpoints occurred most frequently in 10p11 and were mapped within a 1-Mb region in 10p11.2 with heterozygous deletions in all cases. A minimal common region of chromosome deletions, including a region of homozygous deletion, was mapped to a 2-Mb region. Genetic and expression analyses of the genes mapped within the deleted region revealed transcription factor 8 *(TCF8)* to be frequently altered in ATLL cells by several mechanisms, including mainly epigenetic dysregulation, suggesting that *TCF8* may be a candidate tumor suppressor gene. *TCF8* (GenBank accession number, NM 030751[11]), *AREB6, ZFHEP, NIL-2A, ZFHX1A, NIL-2-A, MGC133261,* or

Submitted January 5, 2008; accepted April 4, 2008. Prepublished online as *Blood* First Edition paper, May 8, 2008; DOI 10.1182/blood-2008-01-131185.

*T.H., S.N., and K.H. contributed equally to this paper.

The online version of this article contains a data supplement.

The publication costs of this article were defrayed in part by page charge payment. Therefore, and solely to indicate this fact, this article is hereby marked "advertisement" in accordance with 18 USC section 1734.

ZEB1 encodes a 2-handed zinc finger homeodomain protein,[12] which represents a key player in pathogenesis associated with tumor progression in solid cancers.[13,14] In this study, we found that *TCF8* mutant mice frequently developed $CD4^+$ T-cell lymphoma/leukemia half a year after birth. Furthermore, we showed that down-regulation of TCF8 expression in ATLL cells in vitro was associated with TGF-β1 resistance, a well-known characteristic of ATLL cells, suggesting that escape from TGF-β1–mediated growth inhibition is one of the primary mechanisms in the pathogenesis of ATLL. These findings suggest that *TCF8* has an important tumor suppressor role in ATLL.

Methods

Patient samples

ATLL cells were collected from patients at the time of admission to hospital and before chemotherapy.[15] Diagnosis of ATLL was made on the basis of clinical features, hematologic characteristics, serum antibodies against HTLV-1 antigens, and insertion of the HTLV-1 viral genome into leukemia cells by Southern blot hybridization. Using Shimoyama's criteria,[16] all patients were diagnosed as acute-type ATLL. Mononuclear cells were obtained from heparinized blood or ascites by Histopaque density gradient centrifugation (Sigma-Aldrich, St Louis, MO). After separation, ATLL cell enrichment of more than 90% was confirmed by 2-color flow cytometric analysis. All samples were separated by Histopaque density gradient centrifugation, quickly frozen within 3 hours, and cryopreserved at −80°C. This study was approved by the Institutional Review Board of the Faculty of Medicine, University of Miyazaki. Informed consent was obtained from all blood and tissue donors in accordance with the Declaration of Helsinki.

Cell lines

Acute lymphoblastic leukemia (ALL) cell lines used in this study were described previously.[15] Briefly, 4 of the cell lines, Jurkat, MOLT4, MKB1, and KAWAI, are HTLV-1–negative human T-cell acute lymphoblastic leukemia (T-ALL) cell lines.[17,18] Three cell lines, KOB, SO4, and KK1, are interleukin 2 (IL2)–dependent ATLL cell lines.[19] ED, Su9T, and S1T are IL2-independent ATLL cell lines.[20] MT2 and HUT102 are human T-cell lines transformed by HTLV-1 infection.[21] CTLL2 is a murine IL2–dependent T-lymphoma cell line.[22] All the cell lines were maintained in RPMI1640 medium supplemented with 10% fetal calf serum (FCS) and with or without IL2.

Cell culture and karyotype analysis

G-banding studies were performed as described previously.[8] Briefly, leukemia cells were diluted in 10 mL RPMI1640 medium supplemented with 10% FCS at a final concentration of 10^6 cells/mL. The cells were cultured at 37°C for 24 to 48 hours in humidified air with 5% CO_2, exposed to colcemid (0.05 mg/mL) for 60 minutes, processed in 0.075 M potassium chloride for 20 minutes, and fixed with methanol/glacial acetate (3:1). The chromosomes were treated with trypsin, stained with a Giemsa solution, and karyotyped according to the International System for Human Cytogenetic Nomenclature (ISCN 2005).[23] The remaining chromosome pellets were stored at −20°C for SKY and fluorescence in situ hybridization (FISH) analyses.

SKY and DAPI banding analysis

The strategy of combined spectral karyotyping (SKY) and 4,6-diaminido-2-phenylindole dihydrochloride (DAPI) banding analysis of chromosome abnormalities was published[24] and is briefly described as follows: The chromosomes prepared on a slide glass were denatured and hybridized with a cocktail probe mixture for 2 days at 37°C. The SKY probe mixture and hybridization reagents were purchased from Applied Spectral Imaging (Vista, CA), and signal detection was performed according to the manufacturer's protocol. The chromosomes were counterstained with DAPI combined with an antifade solution (Vectashield; Vector Laboratories, Burlingame, CA). Images were acquired by an SD200 Spectracube (Applied Spectral Imaging) mounted on an Olympus BX50-RF (Olympus, Tokyo, Japan) using a custom-designed optical filter (SKY-1; Chroma Technology, San Diego, CA). With another special optical filter, the inverted DAPI images were captured in conjunction with spectral classifications as QFH band patterns for the identification of chromosomal breakpoints. For each case, 10 to 20 metaphase spreads were analyzed, and karyotypes were described according to the ISCN 2005.[23]

FISH analysis

The plasmid library from sorted human chromosomes 10 (pBS10) was used as a whole chromosome painting (WCP) probe, labeled with digoxigenin-16-dUTP (Boehringer-Ingelheim, Ingelheim, Germany) by standard nick translation. BAC clones were labeled with biotin-16-dUTP (Sigma-Aldrich). Hybridization and signal detection were performed as described previously.[25] A minimum of 50 nuclei was examined for each FISH. FISH analysis was performed on metaphase and interphase chromosomes by 53 BAC clones mapped to the chromosome bands 10p11-12 in the human genome mapping of NCBI (build 36 version 1)[26] as probes.

High-density SNP array comparative genomic hybridization (array-CGH) analysis

Total genomic DNA was digested with *Xba*I, ligated to an adaptor, and subjected to polymerase chain reaction (PCR) amplification using a single primer. After treatment with DNase I, 40 μg of the PCR products was labeled with a biotinylated nucleotide analog and hybridized the microarray. SNP genotypes were scored with the GTYPE 4.1 software (Affymetrix, Santa Clara, CA). Chromosome copy number and LOH were calculated with 2 programs, ACUE 2.1 (Mitsui Knowledge Industry, Tokyo, Japan, http://bio.mki.co.jp/en/product/acue2/index.html) and CNAG 2.0 (Affymetrix).[27] For data normalization, we used 6 normal reference samples. Genomic location of probes on the array was determined with the information in NCBI genome map build 35.1.[26]

Mice

C57BL/6 and ICR mice were purchased from CLEA Japan (Tokyo, Japan) and maintained under specific pathogen-free conditions. The targeted allele of the δ*EF1* gene, the murine orthologue of *TCF8*, lacks only the COOH-proximal zinc finger cluster domain.[28] Approximately 20% of the homozygous *TCF8* mutant mice were born alive and grew up to adulthood, although it was reported to cause a defect in the thymic T-cell development.[28,29] To produce viable homozygous *TCF8* mutant mice, we made their genetic backgrounds more heterogeneous by crossing the C57BL/6 background *TCF8* mutant mice with the ICR outbred strain or F1 (C57BL/6 × C3H) mice.

Assay for cell proliferation

Control siRNA was purchased from Qiagen (Valencia, CA; AllStars Negative Control [ANC] siRNA) and the *TCF8* siRNA was from Ambion (Austin, TX; murine *TCF8;* 5′-CCUGUGGAUUAUGAGUUCA-3′, human *TCF8* 5′-GGGUUACUUGUACACAGCU-3′). For the construction of vectors expressing TCF8, human *TCF8* cDNA was subcloned into pCMV26 (Sigma-Aldrich). The cells were transiently transfected using the Nucleofector Kit (Amaxa, Gaithersburg, MD) according to the manufacturer's recommendations. The transfection efficiency, evaluated by fluorescence microscopy of green fluorescent protein, was more than 80%. Twenty-four hours after transfection, the expression of TCF8 protein in the cells was investigated by Western blotting, while for the cell proliferation studies, each transfectant was plated at a density of 4×10^3 cells per well in 96-well microtiter plates. The cells were treated with various concentrations of transforming growth factor (TGF-β1; R&D Systems, Minneapolis, MN) for 72 hours and counted by the methyl thiazolyl tetrazolium (MTT) assay

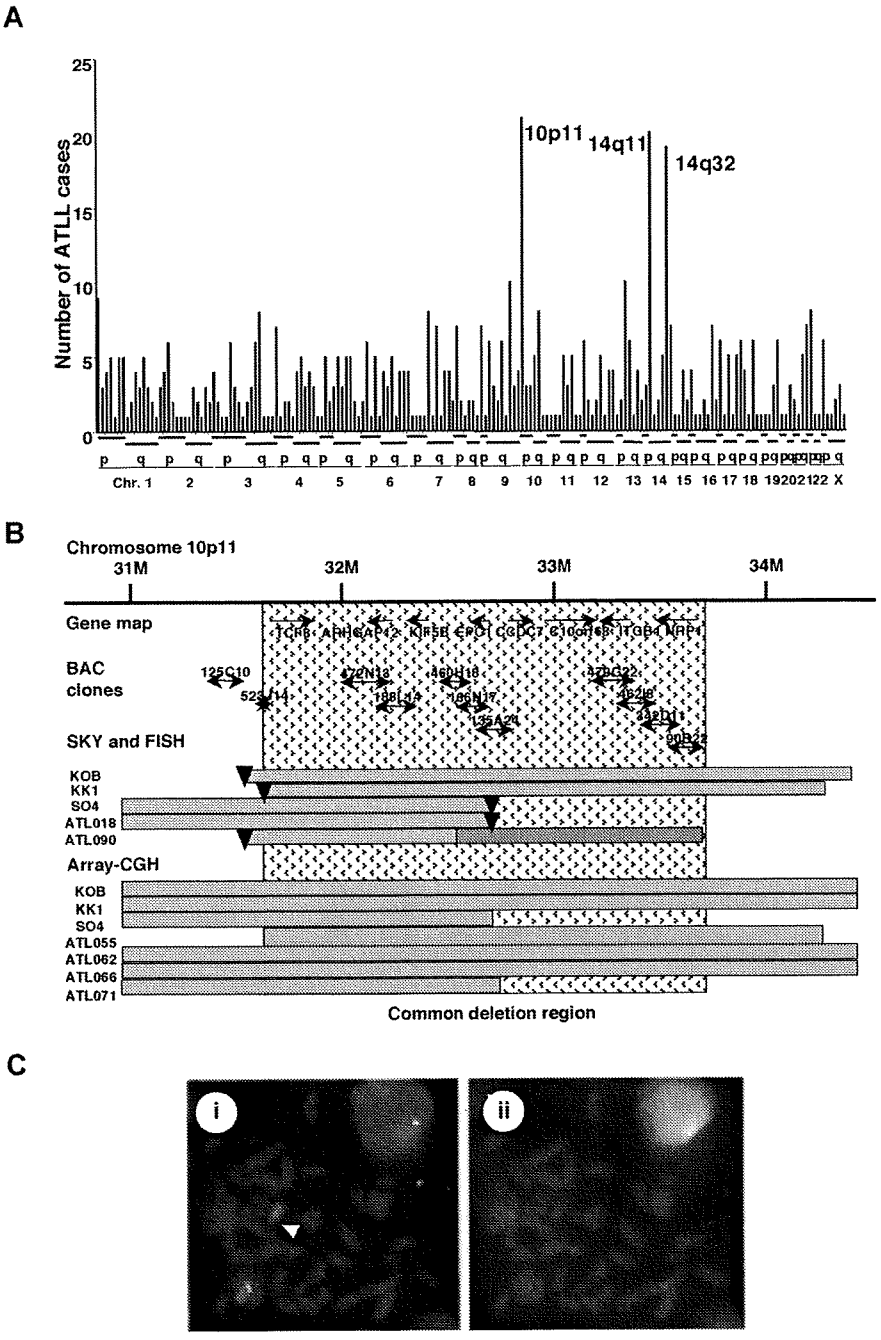

Figure 1. Mapping of the deletions at 10p11.2. (A) Mapping of the chromosomal breakpoints in whole chromosomes in acute-type ATLLs. An analysis of the chromosomal breakpoints was performed by spectral karyotyping (SKY), and all chromosomal breakpoints were mapped in each region of the chromosomes (x-axis), as indicated at the bottom. The y-axis shows the numbers of ATLL cases with the chromosomal breakpoints in each chromosomal region. Three regions, 10p11, 14q11, and 14q32, were frequently identified with chromosomal breakpoints. (B) Physical and transcriptional maps of the region containing the chromosomal deletion at 10p11. A FISH analysis was performed on metaphase and interphase chromosomes using 53 BAC clones mapped to the chromosome bands at 10p11-12 in the human genome map of NCBI (build 36 version 1[26]) as probes. The bars indicate the region covering each BAC clone. Horizontal bars indicate the region with hemizygous deletions in each DNA sample from the ATLL cell lines or ATLL cells from patients, which were detected by SKY and FISH or array-CGH analyses. The inverted triangles indicate the regions of chromosomal breakpoints. Closed bars indicate the region of a homozygous deletion in a DNA sample from ATLL cells (ATL090). The hatch pattern represents the minimal heterozygous deletion at 10p11.2. *TCF8* through *NRP1* represent the names of the genes within the region in the human genome map of NCBI (build 36 version 1[26]). (C) FISH validation of the RP11-188L14 probe to detect the hemizygous deletion of the chromosome10p11.2 in SO4 cell line. The RP11-188L14 probe was green (FITC) and the whole chromosome painting probe was red (TRITC). FISH with RP11-188L14 shows no signal on the abnormal chromosome 10 as indicated by the arrow (i), and a DAPI photograph corresponding to the FISH picture is shown on the right side (ii). Images were captured through the oil objective lens (100×) with a CCD camera (SenSys 0400-GI; Photometrics Ltd, Tucson, AZ). Subsequent image processing was performed with the Software IPLab version 2.4.0 (BD Biosciences Bioimaging, Rockville, MD).

using Tetra color one assay kit (Seikagaku Kogyo, Tokyo, Japan). Each experiment was performed 3 times, and typical results are shown.

Results

Identification of a common hemizygous deletion in 10p11 in ATLL by mapping chromosomal breakpoints

We recently studied recurrent chromosomal rearrangements in adult T-cell leukemia lymphoma (ATLL) cells from 61 patients by spectral karyotyping (T.H. et al, manuscript in preparation). In examining the molecular changes in ATLL cells, 605 chromosomal breakpoints in 61 cases were identified and precisely mapped by DAPI banding analysis. The frequency of the breakpoints was counted in each region of the chromosomes, with an average of around 10 translocations in each case (Figure 1A). Most of the chromosomal translocations were unbalanced, and a few recurrent reciprocal translocations were found. Chromosomal breakages were most frequently identified at 10p11 (21 [34.6%] of 61 cases), and they were also frequently represented at 14q11 and 14q32 regions (Figure 1A). Based on the data of SKY, these 3 events occurred almost independently; however, almost 50% of the cases with 14q32 abnormality demonstrated a 10p11.2 abnormality, suggesting that both events are interrelated chromosomal abnormalities. The 10p11 regions were translocated to more than 10 different partner chromosomal regions, such as 21q22, 13q14, and 14q32.

Therefore, we precisely mapped the chromosomal breakpoints at 10p11 in 3 ATLL cell lines (KK1, KOB, and SO4) and 2 primary ATLL cases (ATL018 and ATL090) by FISH. We identified der(10)t(10,22)(p11.2;q13.1) in KK1, der(10)t(10,14)(p11.2;q11.2)

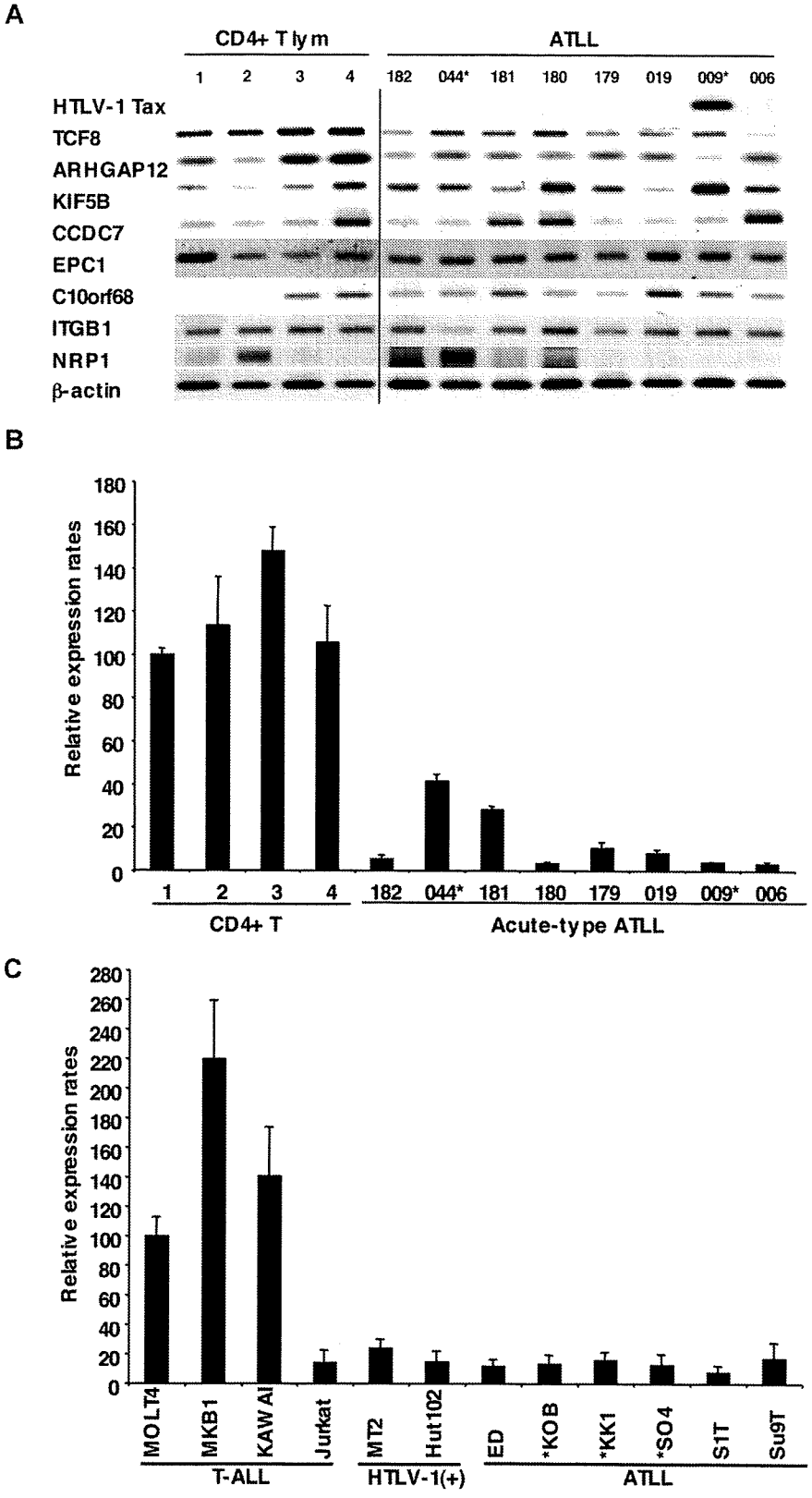

Figure 2. Down-regulated expression of *TCF8* in ATLL cells. (A) The expression profiles of the genes mapped within the deletion region at 10p11. Semiquantitative reverse-transcription PCR (RT-PCR) was performed to determine the expression of the genes mapped within the deletion region. *TCF8, ARHGAP12, KIF5B, CCDC7, EPC1, C10orf68, ITGB1,* and *NRP1* showed a single band of amplified cDNA from $CD4^+$ T lymphocytes from healthy volunteers as controls and from ATLL cells from the patients. A band of HTLV1 *Tax* was amplified from only 1 of 8 ATLL cells. A vertical line has been inserted to indicate a repositioned gel lane. (B) Quantitative RT-PCR analysis of *TCF8* mRNA in 4 samples of $CD4^+$ T lymphocytes from healthy volunteers and 8 samples of ATLL cells from the patients. The data were normalized to *β-actin* mRNA and calibrated to the *TCF8/β-actin* ratio (ΔCT) in the case of healthy volunteer no. 1, as a relative expression rate of 100. The data are the mean and standard deviation of $2^{-\Delta\Delta Ct}$ in a duplicate assay. Two patients (indicated by *) have the chromosome 10p11.2 abnormalities. (C) Quantitative RT-PCR analysis of *TCF8* mRNA in various types of T lymphoblastic leukemia cell lines. MOLT4, MKB1, KAWAI, and Jurkat are T-lymphoid leukemia cell lines; MT2 and HUT102 are HTLV-1–infected cell lines; and ED, KOB, KK1, SO4, S1T, and Su9T are ATLL cell lines. Three ATLL cell lines (indicated by *) showed the deletion of chromosome 10p11.2 with *TCF8*.

in KOB, der(10)t(2,10)(p23;p11.2) in SO4, t(10;21)(p11.2;q11.2) in ATL018, and t(10;13)(p11.2;q14) in ATL090 (Table S1, available on the *Blood* website; see the Supplemental Materials link at the top of the online article). Using 53 BAC clones on 10p as DNA probes for FISH (Table S2), the chromosomal breakpoints in these 5 cases were mapped to a 1-Mb region at 10p11.2 (Figure 1B). It was noted that the genomic deletions surrounding the chromosomal breakpoints were detected by a FISH analysis (Figure 1C) and heterozygous deletions of the 10p11.2 region with translocations were found in all 5 samples (Table S2; Figure 1B). Heterozygous deletions of approximately 2 to 8 Mb in the 10p11.2 region with translocations were found in all 5 samples. In addition, no FISH